Assessing national exposure and impact to glacial lake outburst floods considering uncertainty under data sparsity

Huili Chen[1], Qiuhua Liang[1], Jiaheng Zhao[2], Sudan Bikash Maharjan[3]

[1] School of Architecture, Building and Civil Engineering, Loughborough University, Loughborough LE11 3TU, UK

5   [2] FM Global, 117369, Singapore

[3] International Centre for Integrated Mountain Development (ICIMOD), Nepal

Correspondence to: Qiuhua Liang (Q.Liang@lboro.ac.uk)

Abstract. Glacial Lake Outburst Floods (GLOFs) are widely recognized as one of the most devastating natural hazards in the Himalayas, with catastrophic consequences including substantial loss of life. To effectively mitigate these risks and enhance

10 regional resilience, it is imperative to conduct an objective and holistic assessment of GLOF hazards and their potential impacts over a large spatial scale. However, this is challenged by the limited availability of data and the inaccessibility to most of the glacial lakes in high-altitude areas. The data challenge is exacerbated when dealing with multiple lakes across an expansive spatial area. This study aims to exploit remote sensing techniques, well-established Bayesian regression models for estimating glacial lake conditions, cutting-edge flood modelling technology, and open data from various sources to innovate a framework

15 for assessing the national exposure and impact of GLOFs. In the innovative framework, multi-temporal imagery is utilized with a Random Forest model to extract glacial lake water surfaces. Bayesian models, derived from previous research, are employed to estimate a plausible range of glacial lake water volumes and associated GLOF peak discharges while accounting for the uncertainty stemming from the limited size of available data and outliers within the data. A significant number of GLOF scenarios is subsequently generated based on this estimated plausible range of peak discharges. A graphics processing unit

20 (GPU)-based hydrodynamic model is then adopted to simulate the resulting flood hydrodynamics in different GLOF scenarios. Necessary socio-economic information is collected and processed from multiple sources, including OpenStreetMap, Google Earth, local archives, and global data products, to support exposure analysis. Established depth-damage curves are used to assess the GLOF damage extents to different exposures. The evaluation framework is applied to 21 glacial lakes identified as potentially dangerous in the Nepal Himalayas. The results indicate that Tsho Rolpa Lake, Thulagi Lake, and Lower Barun

25 Lake bear the most serious impacts of GLOFs on buildings, roads and agriculture areas, while Thulagi Lake could influence existing hydropower facilities. Six anonymous lakes (located at 85°37′51″ E, 28°09′44″ N; 87°44′59″ E, 27°48′57″ N; 86°55′41″ E, 27°51′00″ N; 86°51′29″ E, 27°41′13″ N; 86°55′01″ E, 27°49′55″ N; 87°56′05″ N, 27°47′26″ E) have the potential to impact more than 200 buildings. Moreover, anonymous lake (located at 85° 37′ 51″ E, 28° 09′ 44″ N) have the potential to inundate existing hydropower facilities.

30 ## 1 Introduction

Glacial Lake Outburst Floods (GLOFs) are recognized as one of the most impactful natural hazards in the Himalayas, where these disasters have had the highest death toll worldwide and caused serious economic damage (Veh et al., 2020). GLOFs can generate transient discharges that are orders of magnitude greater than the typical annual floods in the receiving rivers (Cenderelli and Wohl, 2001) and some of them can travel >200 km downstream (Richardson & Reynolds, 2000). The extreme

35 discharges, accelerating along the steep mountainous terrains, make GLOFs extremely destructive to downstream communities and infrastructure systems. The unpredictable nature of GLOFs, often occurring without warning, has left downstream communities and infrastructure ill-prepared, causing the loss of human lives and economic damages. The ongoing impact of climate change has introduced additional uncertainty into GLOF risk. The Himalaya region is observing extensive glacier

shrinkage and a proliferation of glacial lakes (Zhang et al., 2015). The potential impacts of GLOFs on downstream communities are expected to intensify further due to population growth and socio-economic development. Hence, it is crucial to develop effective strategies for managing GLOF risks to enhance human safety and support sustainable development. This necessitates the requirement for reproducible assessment of GLOF hazards and their potential impacts arising from these glacial lakes.

Some potentially dangerous lakes have been well-studied individually, such as Tsho Rolpa Lake (e.g., Shrestha & Nakagawa, 2014), Imja Tsho Lake (e.g., Somos-Valenzuela et al., 2015), and Lower Barun Lake (e.g., Sattar et al., 2021). However, these studies provide limited insight into the overall danger and potential impacts of glacial lakes as a whole. While there have been assessments of glacial lake hazards in the Himalayan region, certain limitations exist. Previous work by Mool et al. (2011) and Bajracharya et al. (2020) employed remote sensing techniques to identify potentially dangerous glacial lakes (PDGLs) in Nepal, considering different hazard factors. Rounce et al. (2017) undertook a similar study, quantifying the hazard level of 131 glacial lakes with > 0.1 km^2 area in Nepal. Furthermore, Rounce et al. (2017) evaluated the potential downstream impacts of GLOFs caused by these glacial lakes using a simple flood model without any physical basis. This simple flood model has also been applied to evaluate the overall impacts of GLOFs originating from multiple glacial lakes in the Indian Himalayas (Dubey & Goyal, 2020). Zheng et al. (2021) extended their analysis to assess the impacts of GLOFs across the Third Pole by using a Geographic Information System (GIS)-based hydrological model. However, the complexity of GLOFs renders simple flood models inadequate for capturing their dynamics, thereby making them incapable of supporting detailed assessments of potential impacts on downstream communities and infrastructure.

A range of physically based hydrodynamic models has been developed and applied to predict the spatial-temporal process of GLOFs, offering detailed insights into the resulting flood impacts (e.g., Worni et al., 2014; Ancey et al., 2019; Sattar et al., 2019). Recently, researchers have explored the use of a hydrodynamic model to assess GLOF downstream impacts in the Third Pole (Zhang et al., 2023b). However, hydrodynamic models entail a huge amount of computation and face substantial demands for computation resources when applied at a large scale. What's even more challenging is that the computational requirements increase significantly when addressing GLOF simulations involving a large number of scenarios, which is necessary for assessing GLOF's potential impact due to the complexity and uncertainty of the glacier lake breach process. Moreover, the application of hydrodynamic models to support GLOF modelling and impact assessment necessitates a considerable amount of data, and data availability poses another significant challenge.

The high-alpine conditions have constrained our ability to acquire detailed spatial data for multiple lakes across a large scale. To correctly depict the dynamic inundation process of GLOFs, glacial lake conditions and dam breaching process are essential to estimating the outflow discharge resulting from a breach. While the distribution and changes of glacial lakes have been extensively mapped from increasingly available satellite imagery (e.g., Zhang et al., 2015; Nie et al., 2017; Shugar et al., 2020), accurately determining lake volume and reliably predicting dam breaching processes has remained a challenge because high-alpine conditions impede detailed fieldwork. Combining satellite imagery with existing lake bathymetry measurements offers the possibility of estimating water volumes and peak discharges from outbursts by establishing empirical relationships (e.g., Zhang et al., 2023a). However, estimated lake volumes and potential peak discharges derived from these empirical relationships can vary by up to an order of magnitude (Cook and Quincey, 2015; Muñoz et al., 2020). To account for the uncertainties inherent in conventional empirical relationships, Veh et al. (2020) developed a Bayesian robust regression, utilizing data from the bathymetric survey of 24 glacial lakes. This model estimates water volume based on the surface areas of glacial lakes. Simultaneously, they created a Bayesian variant of a physical dam-break model originally proposed by Walder & O'Connor (1997) to predict peak discharge associated with the estimated flood volume. The Bayesian estimates explore the parameter space of plausible flood volumes and associated peak discharges, generating a million possible outburst scenarios for each lake. These scenarios comprehensively consider all potential conditions of the dam breach process for each specific lake and provide a full range of input information for hydrodynamic models, thereby facilitating predictions of the GLOF

inundation process. Therefore, this study aims to leverage these established Bayesian models to support GLOF inundation simulations.

GLOF exposure and impact assessment are also restricted by data sparsity. Previous studies have typically relied on census data at coarse spatial resolutions or aggregated land use data that encompasses various objects like properties and infrastructure, to estimate the potential socio-economic impact of GLOFs (e.g., Shrestha & Nakagawa, 2014; Rounce et al., 2016). Benefiting from the emergence of new data technologies and the resulting enhancements in data quantity and quality, a spatially explicit assessment method has been developed to identify GLOF exposure at an object level and applied to the Tsho Rolpa Lake (Chen et al., 2022). Employing a similar strategy, essential socio-economic information is collected and processed from various sources, including OpenStreetMap (OSM), Google Earth, global data products, and local archives. The information is used to create a spatial exposure dataset that specifies the locations of different objects, such as individual buildings and hydropower facilities. Subsequently, this spatial exposure data is overlaid with the spatially distributed flood simulation outputs to identify potential exposure to GLOFs along their path.

Overall, this study aims to innovate a framework for object-based exposure and potential impact assessments of GLOFs for multiple lakes across a large scale by exploring the use of remote sensing techniques, the developed Bayesian regression models for estimating lake volumes and potential peak discharges, a physically based hydrodynamic model supported by parallelized high-performance computing, and socio-economic information from multiple sources. Nepal has been chosen as the test area due to its abundance of glacial lakes, and it has been reported to experience the most significant national-level economic consequences from GLOFs globally (Carrivick & Tweed, 2016).

2 Methodology and data

The proposed framework for object-based exposure and impact assessment of GLOFs across multiple lakes comprises several key components: extraction of glacial lake water surfaces from multi-temporal imagery, estimation of lake volumes and peak discharges using well-established Bayesian regression models, utilization of a high-performance hydrodynamic flood model accelerated by graphics processing unit (GPU) technology, and the creation of an exposure dataset sourced from open-source data (Fig. 1). In particular, leveraging multi-temporal imagery availability, a Random Forest model is developed using a set of predictor variables to delineate the maximum extent of glacial lake water surfaces. The plausible range of glacial lake water depths, volumes, and GLOF-induced peak discharges is estimated through existing Bayesian models. A substantial number of GLOF scenarios, encompassing outflow discharge hydrographs through glacial lakes, are sampled and generated based on the plausible range of peak discharges. For each scenario, the resulting outflow discharge hydrograph is employed to drive the GPU-accelerated hydrodynamic model, efficiently simulating the temporal and spatial dynamics of floods. These flood dynamics are then overlaid with the spatial exposure data to identify potential exposure to GLOFs and quantify damage extent by using established depth-damage curves.
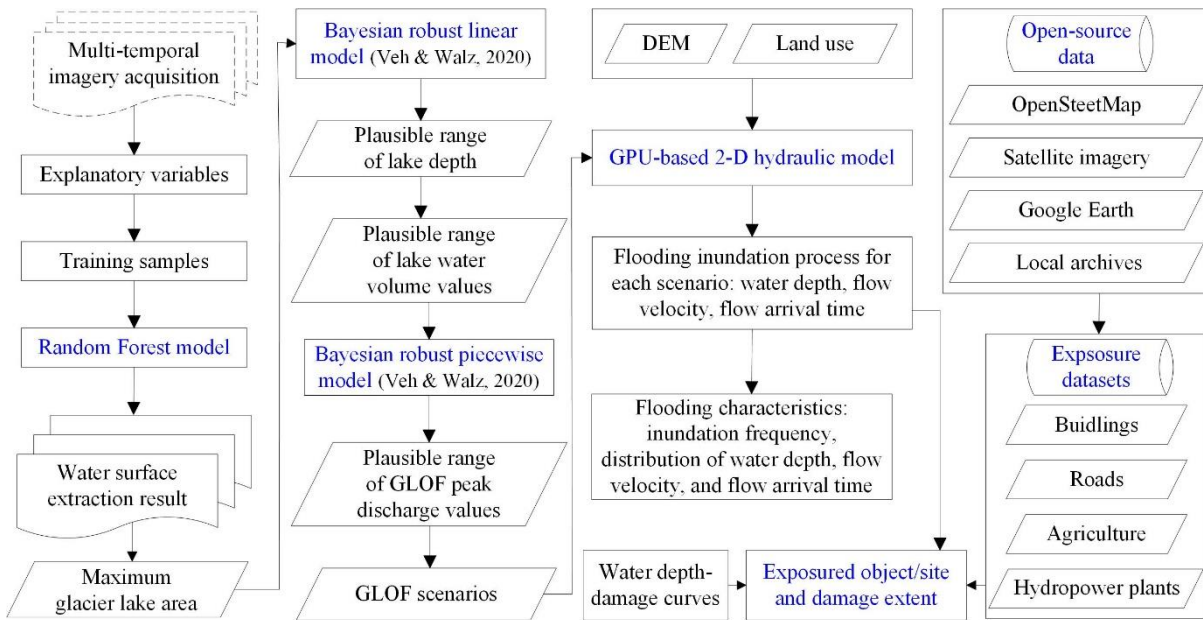
Fig. 1. GLOF exposure and impact assessment framework for multiple glacial lakes (key components highlighted in blue)

2.1 Glacial lake water surface extraction

115 With the availability of multi-temporal imagery, a Random Forest model based on a set of predictor variables is used to map the location and extent of water surfaces of glacial lakes under different hydrological conditions to produce the maximum extent of lake water surfaces.

2.1.1 Acquisition of satellite imagery

Sentinel-2 is an operational multispectral imaging mission of the European Space Agency for global land observation. The
120 Sentinel-2A and -2B satellites were launched in 2015 and 2017, respectively. These satellites capture imagery every 10 days (every 5 days with the twin satellites together). The spatial resolution for the visible and broad near-infrared (NIR) bands is 10m, while it is 20m for the red edge, narrow NIR, and short-wave infrared bands. Here, all available Sentinel-2 imagery for the case study of glacial lakes is utilized to identify the maximum extent of their water surfaces. The analysis is based on the Sentinel-2 level-1C Top-Of-Atmosphere (TOA) products, which are accessible through the Google Earth Engine. Any
125 observations affected by clouds are masked using the Sentinel-2 Quality Assurance band flags. Bands originally at a 20-m resolution are resampled to 10m using the nearest neighbour method before being stacked for subsequent interpretation. All available Sentinel-2 datasets are collected and filtered to reserve imagery from the ablation season, reducing the impact of frozen water surfaces, as per the empirical period of the local melt season (Shugar et al., 2020). In total, 1,520 Sentinel-2 images have been collected for this purpose.

2.1.2 Random Forest model
130

Mapping water surfaces from multiple images is a complex task that necessitates the consideration and analysis of various water-related signals in spectral responses, often influenced by water turbidity and bottom sediments. In this context, a Random Forest model is developed based on a set of predictor variables to extract water surfaces. Random Forest modelling is an ensemble classification technique (Breiman, 2001) and has been extensively used in the classification of remote sensing data
135 (e.g., Yu et al., 2011; Rodriguez-Galiano et al., 2012). Random Forest models excel at recognizing regional variations in threshold values, surpassing the capabilities of traditional index thresholding methods (Tulbure et al., 2016). Notably, Random Forest models do not rely on data distribution assumptions and can yield accurate predictions without overfitting data.

Consequently, they have been increasingly used in water surface extraction as a favourable alternative to traditional statistical approaches (e.g., Schaffer-Smith et al., 2017; Veh et al., 2018).

140   Random Forest model consists of a set of classification trees, each of which grows from a random subset of training samples and randomly permuted explanatory variables. The classification trees can grow to a specified maximum number without pruning, and the final classifications are determined by the majority votes of the trees in the forest. The explanatory variables for Sentinel-2 datasets in the Random Forest model include TOA reflectance for every spectral band, brightness temperature, vegetation indices, and water indices. TOA reflectance and brightness temperature are obtained by normalizing the target

145   imagery, mitigating unwanted effects resulting from variations in sun angle and earth-sun distance. The vegetation indices include the Normalized Difference Vegetation Index (NDVI) and the Enhanced Vegetation Index (EVI). NDVI is sensitive to chlorophyll and used to assess terrestrial vegetation conditions (Tucker, 1979), while EVI is developed to optimize the vegetation signal in high biomass regions, de-couple canopy background signal, and reduce atmospheric influences (Huete et al., 2002). Water indices include the Normalized Difference Water Index (NDWI, McFeeters, 1996), Modified NDWI

150   (MNDWI, Xu, 2006), and Normalized Difference Moisture Index (NDMI, Gao, 1996). NDWI enhances the response to open water features while minimizing soil and terrestrial vegetation influences. MNDWI substitutes the middle infrared band for the NIR band used in the NDWI to enhance water features and remove noise from other land types. NDMI is an effective indicator of vegetation water content. The training samples are selected via visual interpretation of satellite images to represent glacial lake water surfaces, along with various non-water covers, including diverse landscapes and vegetation types. The

155   uncertainty in estimating glacial lake area is quantified using a widely used buffer method (Granshaw and Fountain, 2006). A buffer area of half a pixel (e.g., Zhang et al., 2015; Krause et al., 2019) is adopted to measure the uncertainty in the estimated lake area. The misclassified glacial lake water areas resulting from terrain shadows are eliminated during post-processing through manual exclusion of inaccurately classified regions.

2.2 GLOF dynamic inundation process simulation

160   Using the maximum extent of glacial lake water surfaces, we employ the established Bayesian models to predict glacial lake conditions and the dam breaching process. This allows us to estimate the full range of GLOF outflow discharge through the breach. Subsequently, various GLOF scenarios featuring a range of outflow discharge hydrographs are then sampled to drive the GPU-based hydrodynamic model for the simulation of dynamic flood dynamics resulting from GLOFs.

2.2.1 Estimating volumes and peak discharge of glacial lakes

165   Global samples from glacial lakes have suggested that the water depths for glacial lakes with similar surface areas can vary by one order of magnitude. To estimate water volumes of glacial lakes, we adopted the model that relates lake areas to their maximum depths, which was developed by Veh & Walz (2020). The model was built by compiling the reported lake areas and maximum depths obtained from bathymetric surveys conducted on 24 Himalayan glacial lakes. A Bayesian robust linear regression with a normally distributed target variable (lake depth d) $d \sim N(\mu_d(a), 1/\tau)$ is adopted to account for possible

170   effects of the limited sample size and outliers present in the compiled dataset. The mean $\mu_d(a)$ is calculated below through a linear combination of the input lake area a. The precision τ (the inverse of variance) is gamma-distributed $\tau \sim \Gamma(0.001, \ 0.001)$.

$$\mu_d(a) = \alpha_0 + \alpha_1 a \tag{1}$$

Where a is lake area, intercept $\alpha_0 \sim N(0, \ 10^{-12})$, slope $\alpha_1 \sim N(0, \ 10^{-12})$.

175   We obtained 100 posterior estimates for the lake depth (d) from the Bayesian model for each lake. For each lake, samples inside the 95% highest density interval (HDI) of credible lake depth values are reserved, i.e., 94 lake depth samples for each

lake. In this study, we maintained the same assumption regarding the bathymetry of the glacial lakes as outlined by Veh & Walz (2020). The delineated lake from satellite imagery is circular, and each lake is assumed to have an ellipsoidal bathymetry. Therefore, we obtained 94 estimates of total volume (V_{tot}) for each glacial lake.

$$V_{tot} = (2/3)\, da \tag{2}$$

With regard to estimating peak discharge during dam failure, Veh & Walz (2020) built a Bayesian piecewise robust model to characterize the physically motivated model developed by Walder & O'Connor (1997). The latter model predicts peak discharge Q_p during natural dam failure. In their study, Walder & O'Connor (1997) compiled data from 63 observed natural dam breaks in various settings and identified a constant response of dimensionless peak discharge $Qp*$ when plotted against the dimensionless product η of lake volume and breach rate k. They inferred a model that describes the relationship between peak discharge and lake volume using the dimensionless peak discharge $Qp*$.

$$Q_p{}^* = Q_P g^{-\frac{1}{2}} h^{-\frac{5}{2}} \tag{3}$$

$$\eta = V_O^* k^* \tag{4}$$

Where $V_O^* = V_0 h^{-3}$ represents the dimensionless flood volume, $k^* = k g^{-1/2} h^{-1/2}$ is the dimensionless breach rate, g is the acceleration of gravity, h is breach depth, and V_0 is the released water volume (flood volume). k is the breach rate and subsumes lithologic conditions, the erodibility of the outflow channel, and the breach and downstream valley geometry. h is measured from the final lake surface after dam failure to the initial lake surface. V_0 is the released water volume and depends on h and V_{tot}.

Empirical data support a piecewise regression model in the form $Q_p{}^* = b_0 \eta^{b_1}$ (b_0 and b_1 are the regression parameters) for $\eta < \eta_c$, and $Q_p{}^*$ is constant for $\eta > \eta_c$. Bayesian piecewise linear regression was developed for predicting peak discharge $Q_p{}^*$ from η, the product of breach rate k and released flood volume (Veh & Walz, 2020). The extent of breaching is closely linked to the geometry and material composition of the dam. To account for the most severe GLOFs, the maximum breach depth is considered to reach the marine dam's maximum depth and extend from the dam crest down to the point where the hummocky terrain ends, as determined using high-resolution satellite imagery and DEM data. The dam maximum depth data were requested from and obtained through Bajracharya et al. (2020) and are presented in Table 1. For each lake, we predicted peak discharge Q_p based on a given value of V_{tot} and η using the Bayesian piecewise linear regression model. We generated 100 estimates of the posterior predicted Q_p for each given value of V_{tot} and η. The values of η for individual lakes encompass the assumed flood volumes, and we also considered 100 physically plausible values of the breach rate k based on a log-normal fit to reported breach rates. By multiplying the 94 samples of V_{tot} with the 100 samples of k and 100 samples of Q_p, we ultimately obtained a total of 940,000 scenarios of Q_p per lake. Considering the substantial computational resources required for GLOF inundation simulations in Section 2.2.2, 100 scenarios are selected from the 940,000 Q_p and associated V_0 scenarios per lake using K-means clustering. The K-means algorithm partitions the Q_p and V_0 data into 100 clusters, optimizing intra-cluster homogeneity and inter-cluster heterogeneity. By selecting the data point closest to the centroid of each cluster, the selected scenarios ensure a diverse and representative sampling across the full spectrum of the dataset. The weight of each selected scenario is determined by its occurrence probability, specifically, the proportion of times its peak discharge does not exceed that of other scenarios, relative to the total number of scenarios. A smaller proportion indicates a lower likelihood of occurrence, while a larger proportion indicates a higher likelihood. The weight of each scenario is calculated by dividing the proportion by the total proportion of all possible scenarios. In these simulations, the dam breach hydrograph is assumed to have an isosceles triangle shape, simplifying its derivation from Q_p and V_0. The breach hydrograph then serves as the boundary condition for the hydrodynamic modelling. Although there is some uncertainty, the assumption of an isosceles triangle shape for the dam breach hydrograph aligns with experimental observations (e.g., Morris et al., 2007; Walder et al., 2015; Yang et

al., 2015) and is supported by simulation results from commonly used mechanisms and empirical models (e.g., Yang et al., 2023). Apart from the most severe scenarios, less severe conditions are also considered, where 25%, 50%, and 75% of the maximum dam breach depth are reached.

2.2.2 2-D hydrodynamic modelling

The High-Performance Integrated Hydrodynamic Modelling System (HiPIMS) (Zhao & Liang, 2022) is employed here to simulate the breach hydrograph. HiPIMS develops a fully dynamic model based on the 2-D depth-averaged shallow water equations. The conservative form of the governing 2-D shallow water equations is expressed as follows:

$$\frac{\partial \mathbf{q}}{\partial t} + \frac{\partial \mathbf{f}}{\partial x} + \frac{\partial \mathbf{g}}{\partial y} = \mathbf{s} \tag{5}$$

where t is the time; x and y represent the Cartesian coordinates; $\mathbf{q}$ denotes the flow variable vector; $\mathbf{f}$ and $\mathbf{g}$ are the flux vectors in the x- and y-direction, respectively; and $\mathbf{s}$ is the source term vector. The vector terms are defined as:

$$\mathbf{q} = \begin{bmatrix} h \\ q_x \\ q_y \end{bmatrix} \qquad \mathbf{f} = \begin{bmatrix} q_x \\ uq_x + \frac{1}{2}gh^2 \\ uq_y \end{bmatrix}$$

$$\mathbf{g} = \begin{bmatrix} q_y \\ vq_x \\ vq_y + \frac{1}{2}gh^2 \end{bmatrix} \qquad \mathbf{s} = \begin{bmatrix} 0 \\ -C_f u\sqrt{u^2 + v^2} - gh\frac{\partial z_b}{\partial x} \\ -C_f v\sqrt{u^2 + v^2} - gh\frac{\partial z_b}{\partial y} \end{bmatrix} \tag{6}$$

where h is the water depth; $q_x = uh$ and $q_y = vh$ are the unit-width discharges in the x- and y- directions, respectively; u and v denote the depth-averaged velocities in two Cartesian directions; and z_b is the bed elevation; and C_f is the bed roughness coefficient.

The governing equations outlined above are solved through a shock-capturing finite volume Godunov-type scheme on uniform grids (Zhao & Liang, 2022). The numerical scheme introduces a robust Godunov-type model to deliver precise and stable predictions of overland flow and flooding processes at the catchment scale. This scheme is implemented through a Python and CUDA C hybrid programming framework to achieve multi-GPU and multi-node high-performance computing for large-scale simulations. It's worth noting that the GPU-accelerated model has demonstrated computational efficiency up to ten times greater than its CPU-based counterpart (Smith & Liang, 2013). HiPIMS is set up using the terrain data and roughness data, and it is driven by the breach hydrograph for each scenario, as calculated in Section 2.2.1. Subsequently, the runoff is automatically routed throughout the flow area.

2.3 GLOF exposure and impact assessment

Based on the GLOF inundation process predicted by HiPIMS for each scenario, we can estimate potential flood exposure by superimposing the exposure datasets onto the flood simulation results. In addition to assessing flood exposure, it is imperative to quantify the potential losses and impacts of GLOFs under various conditions to understand the associated risks. Estimating the direct damage to buildings and other exposed objects can be achieved by employing appropriate depth-damage curves that establish the relationship between flood depth and the potential damage. Typically, the damage is quantified as a percentage of the cost required for repairs or replacements. In this study, we utilize depth-damage curves from the HAZUS Flood model to investigate the impact of GLOFs on buildings (Scawthorn et al., 2006). Beyond buildings, GLOFs can also have a significant impact on agricultural lands and roads. We evaluate the damage to agricultural lands and roads caused by GLOFs using the damage curves recommended in a technical report published by the Joint Research Centre of the European Commission

250 (Huizinga et al., 2017). The specific water depth-damage curves for buildings, roads, and agricultural lands used in this study can be referenced in Chen et al. (2022).

2.4 Data

HiPIMS is set up using a digital elevation model (DEM) to represent domain topography and land use data to parameterize domain roughness. It is driven by the out-of-breach flow discharge estimated in Section 2.2.1. The DEM used in this work is
255 Shuttle Radar Topography Mission (SRTM) DEM with a spatial resolution of 30 m (Farr et al., 2007). Land use types are extracted from the Landsat Thematic Mapper imagery from the year 2010, provided by the International Centre for Integrated Mountain Development (ICIMOD, 2020). The roughness of the flow area is represented by the Manning coefficient (n), which is dependent on land use types. The values assigned are 0.15 for forest, 0.035 for arable land, 0.03 for grassland, 0.027 for water surface, and 0.016 for construction land. The Manning coefficients 0.016 to 0.15 were specified based on values provided
260 in earlier hydraulic textbooks or reports (such as Chow, 1959; Barnes, 1967; Arcement and Schneider, 1984), aligning with previous studies, for example, 0.035 to 0.17 in Nepal (Sattar et al., 2021) and 0.035 to 0.120 in Bhutan (Rinzin et al., 2023).

Open-source datasets are used to support the assessment of GLOF exposure and impacts. The OSM is a collaborative user-generated project initiated in 2004 to provide an openly available geographical database of the world, covering both the natural and artificial environments of the Earth's surface (OpenStreetMap contributors, 2015). While primarily built by volunteers,
265 OSM also integrates geographical data contributed by governmental and specialized GIS databases for certain areas or entire countries, e.g., Nepal, providing relatively complete spatial data on buildings and other objects. Hydropower plant data are obtained from the Hydro Map project (Nepal Hydropower Portal, 2019). In the Hydro Map project, hydropower plants are categorized into three types: operation, generation, and survey. In Nepal, the hydropower licensing regime is divided into two stages i.e., a survey license is issued to conduct a feasibility and environmental assessment, and a generation license is granted
270 after the project is found to be technically, environmentally, and economically viable. From the Hydro Map project, Nepal has a total of 572 hydropower projects. These projects include 81 that are currently operational, 180 with issued generation licenses, and 311 with issued survey licenses. Detailed information on each hydropower plant is provided, including capacity, commission/issue date, longitude, latitude, etc. Importing hydropower plant data in ArcGIS and comparing it with sub-meter imagery from ArcGIS Server and Google Earth, the positions of some hydropower plants are found to be inaccurate. To address
275 the inaccuracies in the positions of some hydropower plants, a process has been undertaken to enhance the quality of the hydropower plant data. Initially, we identified all hydropower stations located within a 2 km buffer zone along the downstream rivers of glacier lakes. For licensed hydropower plants that were not situated on the river, we relocated them to the nearest river point, ensuring they were accurately placed on the river as indicated by the Hydro Map project. For operational rivers, we used high-resolution remote sensing imagery from sources such as Google Maps and Google Earth to precisely determine
280 their locations.

3 Study area and glacial lakes

Nepal is highly vulnerable to GLOFs. A total of 53 GLOF events have been documented in Nepal from 1560 to now (Shrestha et al., 2023). Additionally, there have been 37 GLOF events recorded in the Tibetan Autonomous Region, China, that had transboundary impacts on Nepal. These historical events have had devastating consequences for the country. For example,
285 both the 1985 Dig Tsho GLOF and the 1998 Tam Pokhari GLOF had devastating effects, resulting in significant loss of life, property and infrastructure damage, and severe disruptions to the livelihoods of those living in downstream areas. Approximately 1.56 million people live downstream within 3 km of moraine-dammed lakes in Nepal, putting them at risk of GLOFs (Ghimire, 2004). If climate change continues at its present pace, rates of glacier mass loss and shrinkage and the formation and expansion of glacial lakes will increase further, which could escalate the occurrence of GLOFs. Exacerbating

290   the situation, GLOF exposure and risk are on the rise due to the expansion of settlements, economic activities, and infrastructure construction along riverbanks.

In Nepal, a total of 2,070 glacial lakes with lake areas equal to or larger than 0.003 km^2 have been identified and mapped using Landsat images (Bajracharya et al., 2020). These glacial lakes are predominantly situated in northern Nepal, at elevations ranging from 3400m to 5908m. Notably, 98% of these glacial lakes are positioned above 4000m. Bajracharya et al. (2020)

295   assessed GLOF hazard factors related to lake and dam characteristics, glacier activity at the source, and the morphology of the lake surroundings for the 2,070 glacial lakes. They identified 21 lakes as PDGLs (Fig 2 and Table 1). Among the 21 PDGLs, some lakes have names, while others do not and were designated as 'Anonymous'.
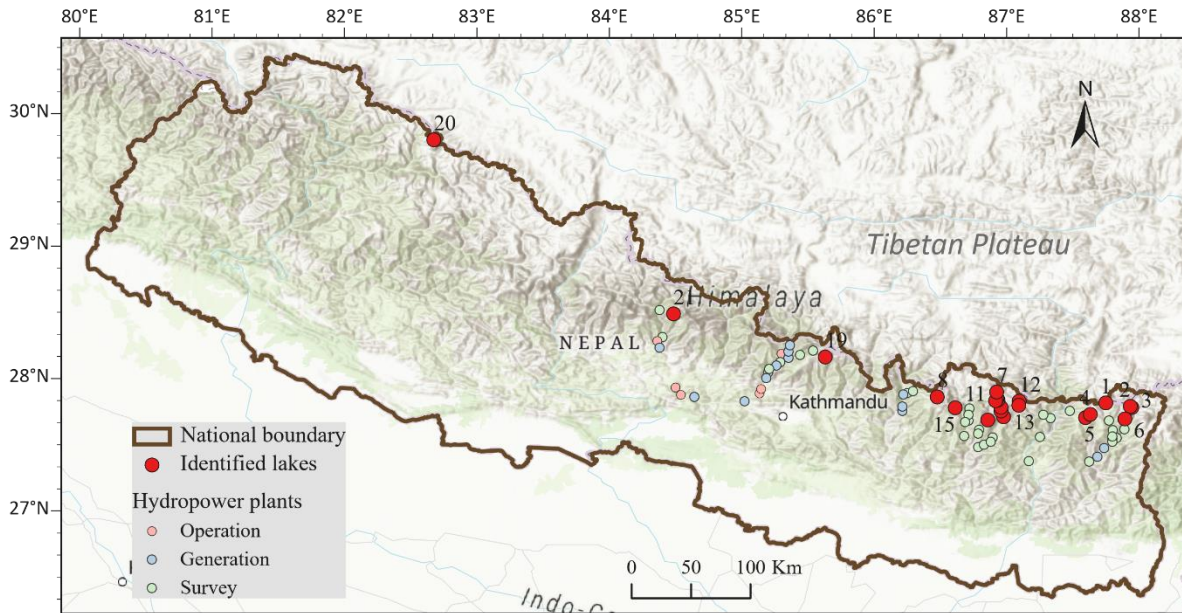
Fig 2. Study area and 21 identified dangerous glacial lakes each with a unique lake number, and potentially impacted hydropower
300   **plants.**

In this study, the focus is on these 21 PDGLs, and a comprehensive assessment of their GLOF risk and downstream impacts is conducted. Each lake is assessed using the proposed evaluation framework in Section 2. The model and evaluation domain for each lake are determined based on the maximum potential inundation extent resulting from GLOFs, as well as the topographic features and river network conditions downstream. Typically, the domain spans more than 100 km and is

305   sufficiently extensive to encompass all potential impacts.

Table 1 Delineated glacial lake areas under varied water-occurrence frequency from multi-temporal Sentinel-2 imagery

Lake number	Lake ID	Lake name	Maximum depth of dam (m)	Longitude (E)	Latitude (N)	Area (km²) (> 5%)	Area (km²) (> 25%)	Area (km²) (> 50%)
1	GL087749E27816N	Anonymous 1	221	87°44′59″	27°48′57″	0.178 ± 0.011	0.169 ± 0.011	0.161 ± 0.011
2	GL087934E27790N	Anonymous 2	128	87°56′05″	27°47′26″	0.148 ± 0.012	0.134 ± 0.012	0.112 ± 0.010
3	GL087945E27781N	Anonymous 3	124	87°56′42″	27°46′51″	0.048 ± 0.005	0.040 ± 0.005	0.035 ± 0.004
4	GL087632E27729N	Anonymous 4	63	87°37′55″	27°43′44″	0.036 ± 0.004	0.032 ± 0.004	0.016 ± 0.005
5	GL087596E27705N	Anonymous 5	158	87°35′46″	27°42′18″	0.026 ± 0.003	0.020 ± 0.003	0.010 ± 0.003
6	GL087893E27694N	Anonymous 6	51	87°53′36″	27°41′41″	0.037 ± 0.005	0.028 ± 0.005	0.015 ± 0.004
7	GL086925E27898N	Imja Tsho	55	86°55′30″	27°53′53″	1.741 ± 0.047	1.630 ± 0.042	1.561 ± 0.041
8	GL086476E27861N	Tsho Rolpa	159	86°28′34″	27°51′40″	1.712 ± 0.043	1.657 ± 0.041	1.610 ± 0.040
9	GL086928E27850N	Anonymous 7	45	86°55′41″	27°51′00″	0.553 ± 0.021	0.533 ± 0.021	0.510 ± 0.022
10	GL086935E27838N	Hongu 1	43	86°56′06″	27°50′17″	0.322 ± 0.018	0.305 ± 0.018	0.293 ± 0.018
11	GL086917E27832N	Anonymous 8	128	86°55′01″	27°49′55″	0.361 ± 0.015	0.342 ± 0.014	0.332 ± 0.014
12	GL087095E27829N	Anonymous 9	61	87°05′42″	27°49′44″	0.118 ± 0.008	0.114 ± 0.008	0.037 ± 0.012
13	GL087092E27798N	Lower Barun	128	87°05′31″	27°47′53″	2.193 ± 0.048	2.044 ± 0.046	1.900 ± 0.053
14	GL086957E27783N	Hongu 2	382	87°57′25″	27°46′59″	0.872 ± 0.030	0.865 ± 0.030	0.843 ± 0.030
15	GL086612E27779N	Lumding	62	86°36′43″	27°46′44″	1.475 ± 0.037	1.411 ± 0.034	1.349 ± 0.035
16	GL086958E27755N	Chamlang	212	86°57′29″	27°45′18″	0.921 ± 0.027	0.856 ± 0.021	0.700 ± 0.026
17	GL086977E27711N	Anonymous 10	129	86°58′37″	27°42′40″	0.085 ± 0.007	0.074 ± 0.007	0.009 ± 0.003
18	GL086858E27687N	Anonymous 11	172	86°51′29″	27°41′13″	0.336 ± 0.015	0.324 ± 0.015	0.307 ± 0.014
19	GL085630E28162N	Anonymous 12	223	85°37′51″	28°09′44″	0.150 ± 0.009	0.137 ± 0.008	0.124 ± 0.008
20	GL082673E29802N	Anonymous 13	99	82°40′27″	29°48′09″	0.047 ± 0.006	0.041 ± 0.005	0.032 ± 0.005
21	GL084485E28488N	Thulagi	192	84°29′06″	28°29′17″	0.997 ± 0.032	0.964 ± 0.032	0.921 ± 0.029

4 Results

4.1 Glacial Lake Water Surface Extraction

310 Water surfaces of glacial lakes are delineated from Sentinel-2 images using the Random Forest model, as previously outlined. The Random Forest model is trained with a set of training samples that comprise both water and non-water features. To account for seasonal variations in lake water surfaces, the training samples for water features are manually selected from images acquired at different times. Various non-water features encompass diverse landscapes and vegetation types. This training dataset is subsequently employed to drive and train the Random Forest model, which is then employed to delineate water

315 surfaces for all the adopted Sentinel-2 images. The subsequent analysis involves the computation of water-occurrence frequency based on multi-temporal water surfaces. The outcomes of water-occurrence frequency for specific representative lakes are visually presented in Fig. 3. It is noteworthy that lake areas are not consistently characterized by open water throughout the year. For instance, lake 'Anonymous 1' (87° 44′ 59″ E, 27° 48′ 57″ N) (Fig. 3(b)) exhibits an average water-occurrence frequency of 72%, while lake 'Anonymous 2' (87° 56′ 05″ E, 27° 47′ 26″ N) (Fig. 3(d)) has an average

320 water-occurrence frequency of 58%. In contrast, for certain lakes, like 'Anonymous 8' (86° 55′ 01″ E, 27° 49′ 55″ N) and the Tsho Ropla Lake, lake areas are always covered with water. Hence, the capacity to map glacial lakes to assess the associated GLOF risk is influenced by the timing of image acquisition.

Table 1 presents the determined lake areas based on varying water-occurrence frequencies. To mitigate the effects of misinterpretations, such as cloud shadows, a 5% threshold is utilized to exclude areas characterized by low water-occurrence

325 frequencies. Subsequently, the maximum lake boundary is delineated for each lake, allowing for the straightforward calculation of maximum lake areas. Among the 21 lakes, the largest one is Lower Barun Lake, a substantial glacial lake in Nepal known for its depth and size. Its area measures 2.193 ± 0.048 km^2, while the smallest lake (Anonymous 5; 87° 35′ 46″ E, 27° 42′ 18″ N) covers only 0.026 ± 0.003 km^2. Lower Barun Lake, along with the second largest PDGL, Imja Tsho Lake, has undergone significant area growth. The estimated maximum area of Imja Tsho Lake here is 1.741 ± 0.047 km^2. Tsho Rolpa

330 Lake boasts a maximum area estimated at 1.712 ± 0.043 km^2. This aligns with previous findings, which reported that the lake had an area of 0.23 km^2 in 1957, which grew to 1.02 km^2 in 1979, 1.65 km^2 in 1999, and 1.61 km^2 in 2019 (Chen et al., 2021). Lumding Lake, another PDGL with an estimated area exceeding 1 km^2, displayed notable growth. It had an area of 0.104 km^2 in 1963, 0.66 km^2 in 1987, 0.8 km^2 in 1996, and 1.18 km^2 in 2016 (Khadka et al., 2019). Our assessment indicates that the maximum area of Lumding Lake is 1.475 ± 0.037 km^2. In summary, the estimated maximum lake areas derived from multi-

335 temporal satellite images for these extensively studied lakes are in good agreement with previous research. To establish the maximum lake boundary for potential risk assessment, it is imperative to leverage multi-temporal imagery capturing various hydrological conditions of glacial lakes.

The maximum areas of the four large lakes (Lower Barun, Imja Tsho, Tsho Rolpa, and Lumding), each exceeding 1 km^2, are approximately 1.1 times the extent to which water covers more than 50% of the time. In contrast, for the comparatively smaller

340 lakes (Anonymous 3, 4, 5, 6, 10, and 13), the ratio of maximum area to the area covered by water for more than 50% of the time can be as high as 1.4 to 2.5 times. For instance, 'Anonymous 10' (86° 58′ 37″ E, 27° 42′ 40″ N) has a maximum area of 0.085 km^2, while only 0.009 km^2 is covered with water for more than 50% of the time. The areas of small PDGLs exhibit more significant variations in space and time compared to those of larger PDGLs, making the associated risks more uncertain.

345
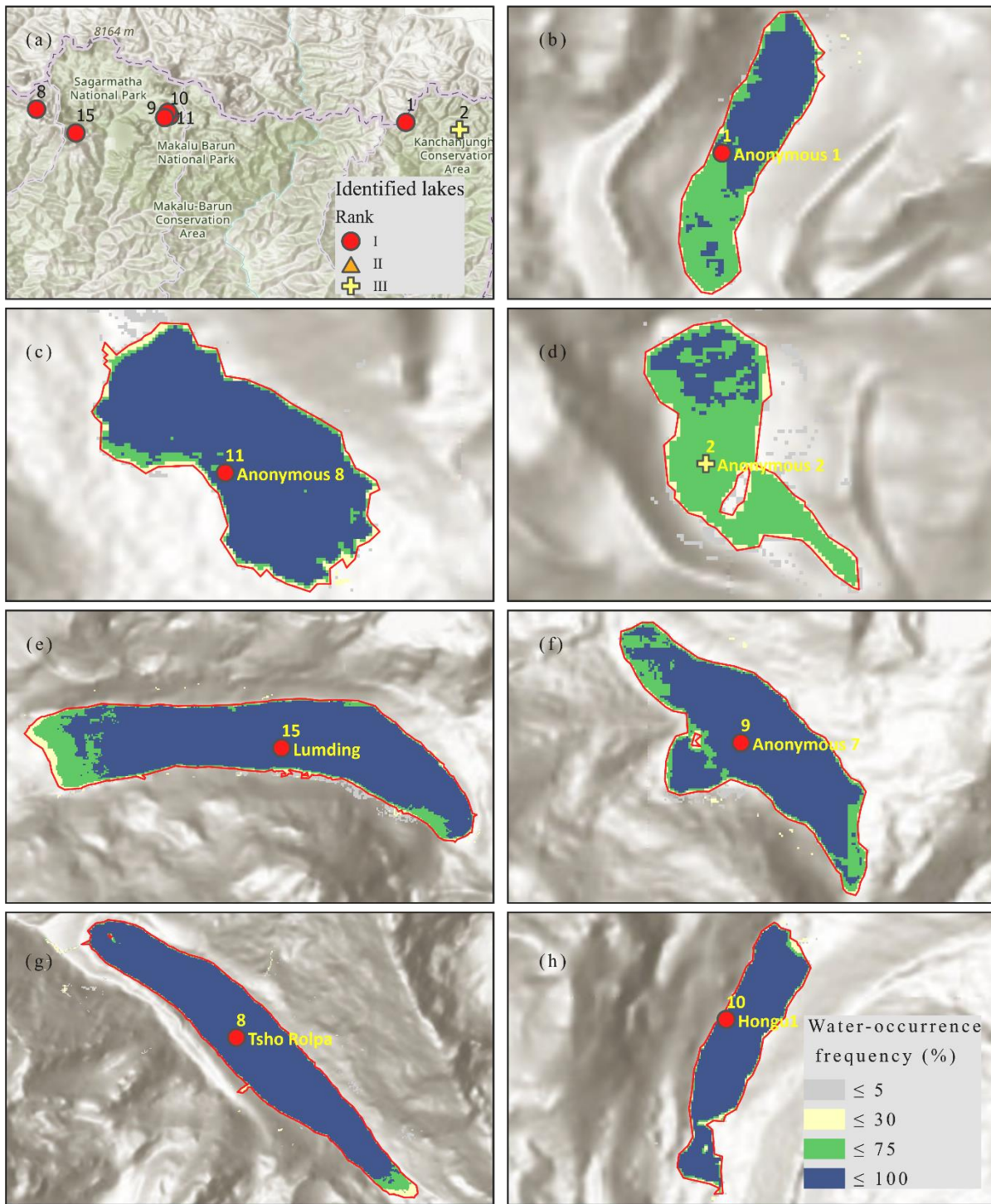
Fig 3 Water surfaces extracted from multi-temporal Sentinel-2 imagery in representative glacial lakes in Nepal (lake numbers and other lake details can be found in Table 1)

4.2 Lake volumes and peak discharges prediction

We obtained 94 estimates of the total volume V_{tot} (Fig 4 (a)) and flood volume V_0 (Fig 4 (b)) for each lake and a total of 940,000

350   scenarios of peak discharge Q_p per lake (Fig 4 (c)) using the models introduced in Section 2.2.1. Figure 4 (a) clearly illustrates

the variation in total volumes among the 21 PDGLs, with Lower Barun (Number 13) standing out as the most substantial,

possessing a median value of approximately 208.2×10^6 m³. In contrast, Anonymous 5 (Number 5) is the smallest, with a

median volume of approximately 204.0×10^3 m³. The disparity between these two lakes is striking, as Lower Barun's median

volume is approximately 1000 times greater than that of Anonymous 5. We collected geophysical investigation data for named

355   PDGLs and compared them against calculated volumes using field-investigated lake areas, as shown in Table 2. While there

are some inconsistencies, the calculated volumes generally align with the investigated values. For example, the water volume of the Lower Barun glacial lake in 2015 was approximately 112.3×10^6 m^3, with a lake area of 1.52 km^2 based on bathymetric measurements. Using the established relationship between lake area and volume, the average volume for a lake with a 1.52 km^2 area is calculated to be 108.27×10^6 m^3, which closely matches the measured volume of the Lower Barun glacial lake.

360   Figure 4 (b) highlights the substantial variation in potential flood volumes across the lakes under the most extreme scenarios, with Lower Barun exhibiting the highest median flood volume, while Anonymous 5 has the lowest. Notably, the median flood volume of Lower Barun is approximately 1,160 times greater than that of Anonymous 5. According to Figure 4(c) showing the distribution of peak discharges, Lower Barun has the highest median peak discharge at 21.3×10^3 m³/s. Following it are Lumding, Imja Tsho and Tsho Rolpa, which have similar peak discharge magnitudes ranging from 13,000 to 15,000 m³/s. The

365   lake with the lowest peak discharge is Anonymous 6, with a discharge of 154.1 m³/s. The peak discharge of Lower Barun is approximately 140 times greater than that of Anonymous 6.
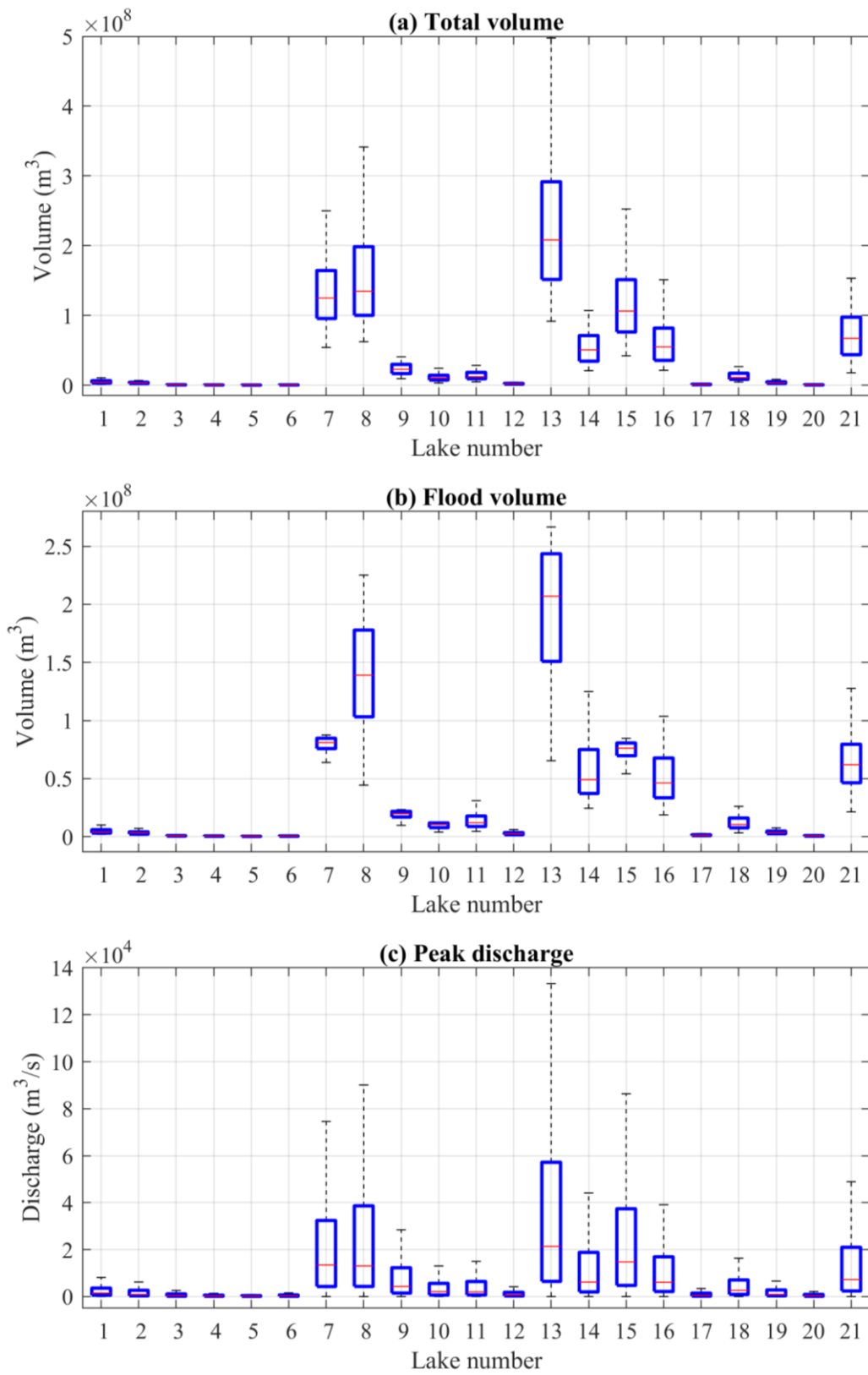
Fig 4 (a) Estimated total volume, (b) flood volume and (c) peak discharge for each glacial lake

Table 2 Comparisons between the lake areas (km^2) and volumes (10^6*m^3) derived from bathymetric investigations and those calculated in this study for named lakes.

Lake number	Lake name	Maximum areas	Median estimated volume	Investigation year	Investigated areas	Investigated volume	Calculated volume for the investigated areas	Reference
7	Imja Tsho	1.741	124.9	2016	1.35	88	87.6	Lala et al., (2017)
8	Tsho Rolpa	1.712	134.7	1994	1.39	76.45	92.1	Rana et al., (2000)
13	Lower Barun	2.193	208.2	2015	1.52	112.3	108.3	Haritashya et al., (2018)
15	Lumding	1.475	106.2	2015	1.13	57.7	65.9	Rounce et al., (2016)
16	Chamlang	0.921	54.9	2009	0.87	34.9 - 35.6	45.8	Lamsal et al., (2016)
21	Thulagi	0.997	67.1	2017	0.89	36	47.1	Haritashya et al., (2018)

370

4.3 Flood inundation simulation

4.3.1 Inundation areas

HiPIMS is used to simulate flood dynamics in 100 scenarios for each lake with maximum dam depth breached. The final flood inundation probability and maximum water depth are derived from each scenario's results multiplied by their respective weight.

375 Herein, we use the simulation results from Imja Tsho Lake and Lower Barun Lake as illustrative examples (Fig. 5). The areas with high flood inundation probabilities are predominantly distributed along the downstream valley. The areas with flood inundation frequency exceeding 5% can be substantial, reaching 95.6 km^2 for Imja Tsho Lake and 200.4 km^2 for Lower Barun Lake. The maximum water depth offers spatial insights into the potential severity of GLOFs in downstream areas (Fig. 5(c) and 5(d)). It facilitates the identification of areas characterized by both high inundation probability and significant maximum

380 water depth. For instance, concerning Lower Barun Lake, there are 127.4 km^2 of areas exhibiting both inundation frequency exceeding 90% and maximum water depth exceeding 0.5 m. These specific areas should undoubtedly receive heightened attention in future flood risk management and mitigation.
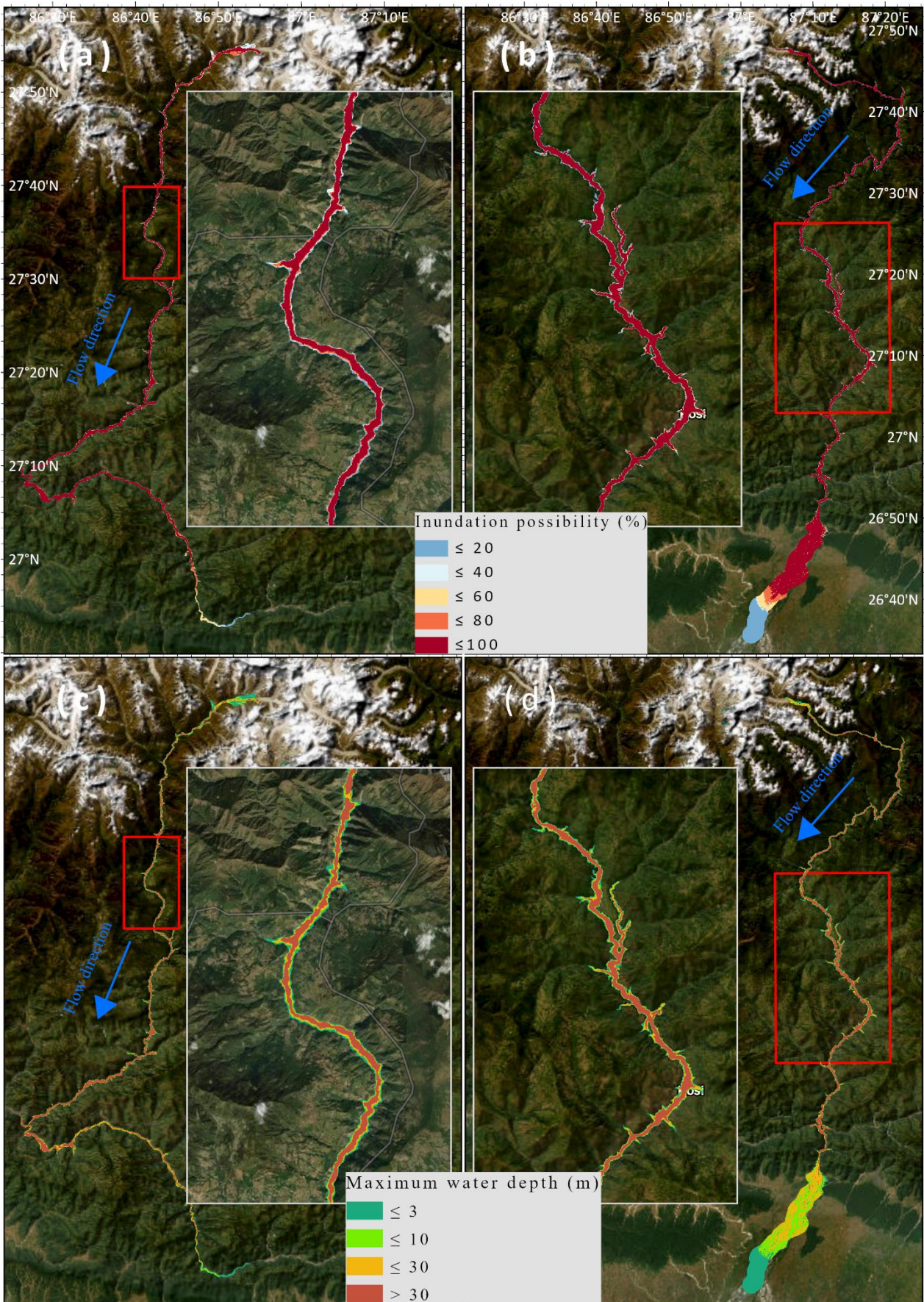
Fig 5 GLOF inundation probability for (a) Imja Tsho Lake and (b) Lower Barun Lake, and maximum water depth for (c) Imja Tsho Lake and (d) Lower Barun Lake under respective worst situation i.e., all lake water will be released. (The basemaps used were accessed from ArcGIS Online Basemap provided by Esri.)

385

The resulting inundation areas at different levels of inundation probabilities are shown in Fig. 6. The inundation extent resulting from GLOFs originating from the 21 PDGLs ranges from 3.6 km² to 200.4 km². Notably, the largest glacial lake, Lower Barun (lake number 13), has an inundation area of 172.4 km² and 189.5 km² for inundation probabilities exceeding 75% and 50%, respectively. Tsho Rolpa (lake number 8), having a smaller lake area than Lower Barun, projects inundation areas of 106.9 km² and 120.3 km² for probabilities exceeding 75% and 50%, respectively. Imja Tsho Lake (lake number 7), similar in size to Tsho Rolpa Lake, anticipates inundation areas of 67.2 km² and 79.6 km² for probabilities exceeding 75% and 50%, respectively. It is worth noting that lakes that have not been extensively studied can potentially cause large inundation areas of over 10 km² for probabilities exceeding 50%, including Anonymous 7 (86° 55′ 41″ E, 27° 51′ 00″ N), Anonymous 8 (86° 55′ 01″ E, 27° 49′ 55″ N), Anonymous 11 (86° 51′ 29″ E, 27° 41′ 13″ N), Anonymous 12 (85° 37′ 51″ E, 28° 09′ 44″ N), Anonymous 1 (87° 44′ 59″ E, 27° 48′ 57″ N), and Anonymous 2 (87° 56′ 05″ E, 27° 47′ 26″ N). The smallest lake, Anonymous 5 (87° 35′ 46″ E, 27° 42′ 18″ N), has an inundation area of 2.7 km² for probabilities exceeding 50%.
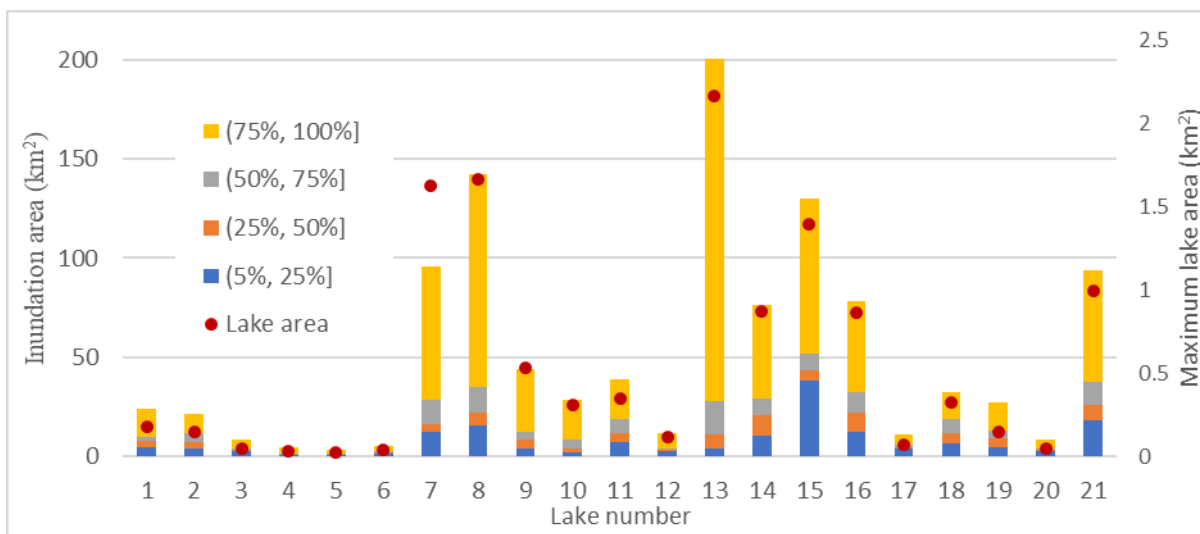
Fig 6 Inundation area (km²) at different levels of inundation probabilities and maximum lake area (km²)

To comprehensively evaluate all potential glacial lake outburst scenarios, we also consider less severe conditions, specifically where 10%, 30%, and 50% of the maximum breach depths are reached. In each of these scenarios, 100 representative cases are selected from a total of 940,000 samples using K-means clustering. The outcomes of these less severe scenarios are then compared to the worst-case conditions. Figure 7 illustrates the inundation areas for probabilities exceeding 5% due to GLOFs. For Lower Barun Lake, breaches reaching 10% and 25% of the maximum breach depth result in inundation of 25.5 km² and 131.0 km² of downstream areas, respectively. When 100% of the maximum breach depth is reached, the inundation areas are 7.87 and 1.53 times larger than those observed in the 10% and 30% maximum breach depth scenarios, respectively. Following Lower Barun Lake, Tsho Rolpa Lake and Lumding Lake also present substantial inundation risks. Even at 10% of the maximum breach depth, Tsho Rolpa Lake has the potential to inundate approximately 40 km² of areas with inundation probabilities exceeding 5%.
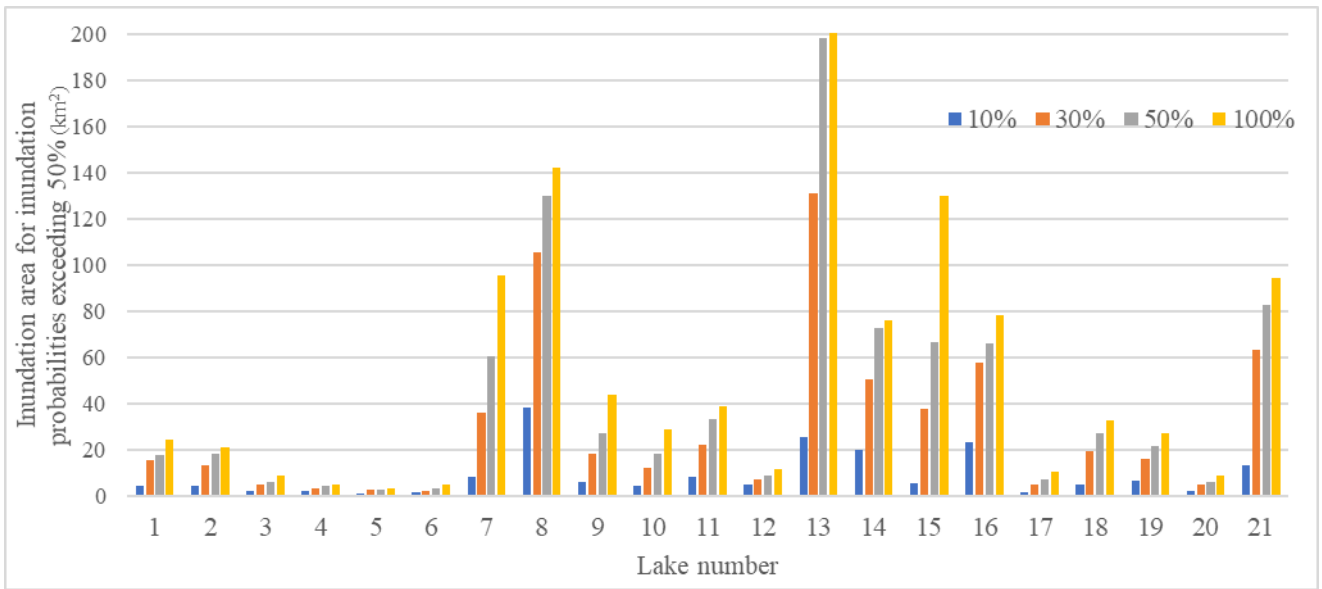
Fig 7 Inundation area (km^2) for inundation probabilities exceeding 5% under 10%, 30%, 50% and 100% of maximum dam depth reached

Table 3 GLOF induced inundation areas and damage extents to buildings, roads, and agricultural lands

Lake name	Area for inundation probabilities > 5% (km^2)	Building number			Building area (m^2)			Road (km)			Agriculture land (km^2)		
		Slight	Moderate	Substantial	Slight	Moderate	Substantial	Slight	Moderate	Substantial	Slight	Moderate	Substantial
Anonymous 1	24.3	37	184	89	1632	11398	4155	8	4	59	1.0	1.1	7.4
Anonymous 2	21.3	46	135	56	2416	8237	3338	10	5	52	0.8	0.9	5.4
Anonymous 3	8.8	9	30	15	818	1990	984	11	3	22	0.7	0.2	0.2
Anonymous 4	4.8	0	8	12	0	360	564	2	1	13	0	0	0
Anonymous 5	3.6	0	14	4	0	685	151	1	0	3	0	0	0
Anonymous 6	5.0	8	5	2	487	246	58	6	1	15	0.5	0.1	0.2
Imja Tsho	95.6	84	418	1165	3827	27148	73595	13	9	194	1.2	1.3	26.4
Tsho Rolpa	142.2	94	1155	7394	3988	63149	407551	17	25	605	1.1	3.3	67.4
Anonymous 7	44.2	19	86	178	699	3778	9956	4	2	49	0.5	0.5	9.9
Hongu 1	28.9	15	76	34	484	4533	1019	2	2	27	0.5	0.4	6.4
Anonymous 8	39.0	37	141	95	1339	6783	6062	6	4	43	0.7	0.8	9.0
Anonymous 9	11.5	2	3	6	60	111	339	4	2	19	0.3	0.1	0.3
Lower Barun	200.4	149	1685	3194	8189	168565	185868	8	8	336	0.6	1.0	70.9
Hongu 2	76.3	60	394	612	2533	15081	26779	14	12	144	1.1	2.3	25.0
Lumding	130.0	26	292	1167	1022	11977	54413	7	7	195	0.7	1.8	34.9
Chamling	78.5	41	412	658	1395	16213	28405	11	12	151	0.7	2.5	26.6
Anonymous 10	10.8	1	0	10	61	0	177	1	1	2	0.6	0.6	0.8
Anonymous 11	32.7	37	135	108	1215	6364	6930	5	4	37	0.7	0.8	9.5
Anonymous 12	27.2	320	964	375	29096	97711	32754	26	13	89	1.7	1.8	6.9
Anonymous 13	8.7	9	20	0	470	1168	0	15	6	12	0.1	0	0
Thulagi	94.2	530	5340	6520	34873	335010	529555	45	44	450	2.4	4.2	46.8

415

4.3.2 Exposure assessment

The exposure of objects can be spatially determined by overlaying the predicted flood inundation maps with relevant datasets detailing buildings, roads, and agricultural land (Table 3). Here, we focus on areas with flood probabilities greater than 5%. The number of inundated buildings varies from 11 to 34,715. Out of the 21 PDGLs, 14 lakes have a number of inundated buildings exceeding 100, while 8 of them inundate at least 1,000 buildings. The three lakes with the highest number of inundated buildings are Thulagi, Tsho Rolpa, and Lower Barun, each of which could inundate more than 5,000 buildings and cover an area of 3.7×10^5 m² of building areas. The number of buildings inundated by Tsho Rolpa and Thulagi is 1.7 and 2.5 times that of Lower Barun Lake, respectively. Overall, these well-studied lakes could impact more buildings than anonymous lakes. These 13 anonymous lakes typically affect fewer than 300 buildings, with the exceptions being Anonymous 1 (87° 44′ 59″ E, 27° 48′ 57″ N) and Anonymous 12 (85° 37′ 51″ E, 28° 09′ 44″ N), which can influence 310 and 1,659 buildings, respectively. Six anonymous lakes including Anonymous 12, 1, 7, 11, 8 and 2 have the potential to impact more than 200 buildings. Further investigation and research are required for the six anonymous lakes. Conversely, three lakes, including Anonymous 10 (86° 58′ 37″ E, 27° 42′ 40″ N), Anonymous 6 (87° 53′ 36″ E, 27° 41′ 41″ N), and Anonymous 9 (87° 05′ 42″ E, 27° 49′ 44″ N), pose lower risks, with a number of 15 or fewer buildings affected.

Regarding inundated roads, the value ranges from 4 to 646 km. Tsho Rolpa, Thulagi Lake, and Lower Barun still hold the top three positions with the largest lengths of inundated roads, each exceeding 350 km. To illustrate, Tsho Rolpa Lake, the top one in this category, inundates a 646 km long road. Following closely is Thulagi Lake, which has inundated roads with a length of 539 km. Agriculture is a cornerstone of the Nepalese economy, and it is susceptible to the impacts of GLOFs. It is anticipated that twelve lakes have more than 10 km² of inundated agricultural land, while three lakes have a negligible impact on agriculture. Lower Barun, Tsho Rolpa, and Thulagi are still the most perilous lakes concerning the inundation of agricultural lands.

In addition to the high potential for human settlements to be exposed to GLOFs, hydropower projects are increasingly vulnerable to these events. A total of 49 hydropower plants (as shown in Figure 2, with detailed information provided in the supporting document Table S1) have been identified as being in close proximity to GLOF flow channels, thereby rendering them potentially vulnerable to GLOFs associated with the 21 PDGLs. Among these, 5 plants are currently operational. Additionally, 44 hydropower plants, for which generation or survey licenses have been issued, are also exposed to the risk of GLOFs from these 21 PDGLs. When examining the potential impact of lakes on operational hydropower plants and those holding generation licenses, it is observed that Thulagi and Tsho Rolpa pose a risk of inundating 5 plants (3 operational and 2 licensed) and 3 plants (all licensed), respectively. Moreover, it is noteworthy that lakes Anonymous 12, Anonymous 1, and Anonymous 2 have the potential to inundate 7 plants (2 operational and 6 licensed), 2 plants (both licensed), and 2 plants (both licensed), respectively.

4.3.3 Damage Assessment

GLOF damage assessment relies on spatial inundation maps of water depth and depth-damage curves. The inundation maps, depicting water depth, are represented by maximum water depths, for areas with flood probabilities greater than 5%. Following the technical manual of the HAZUS Flood model (FEMA, 2009), damage extents of 1% to 10%, 11% to 50%, and 50% to 100% are defined as slight, moderate, and substantial damage, respectively. Figure 8 uses Lake Anonymous 12 as an example to illustrate the spatial distribution of damage to buildings, roads, and agricultural land caused by GLOFs. Table 3 provides estimates of damage to buildings, roads, and agricultural lands for each lake. In the case of Tsho Rolpa, 7,394 buildings are projected to suffer substantial damage from GLOFs. Thulagi Lake and Lower Barun Lake are expected to cause substantial

455 damage to 6,520 and 3,194 buildings, respectively. Other lakes, such as Imja Tsho Lake and Lumding Lake, are estimated to impact roughly 1,160 buildings with substantial damage. Notably, Anonymous 12 (85° 37′ 51″ E, 28° 09′ 44″ N) has the potential to affect 1,659 buildings, with 964 experiencing moderate impact and 375 facing substantial damage. Situated in the Trishuli River Basin, Anonymous 12 faces high exposure. On the other hand, another anonymous lake (Anonymous 13, at 82° 40′ 27″ E, 29° 48′ 09″ N) is not projected to cause any substantial damage to buildings due to GLOFs. For PDGLs

460 with a high number of impacted buildings (more than 1,000), except for Anonymous 12, more than 50% of the impacted buildings are expected to incur substantial damage. In all PDGLs, most affected buildings (over 60%) are predicted to experience moderate or substantial damage. Likewise, over 60% of roads and agricultural lands are anticipated to undergo moderate or substantial damage due to high levels of maximum water depth.
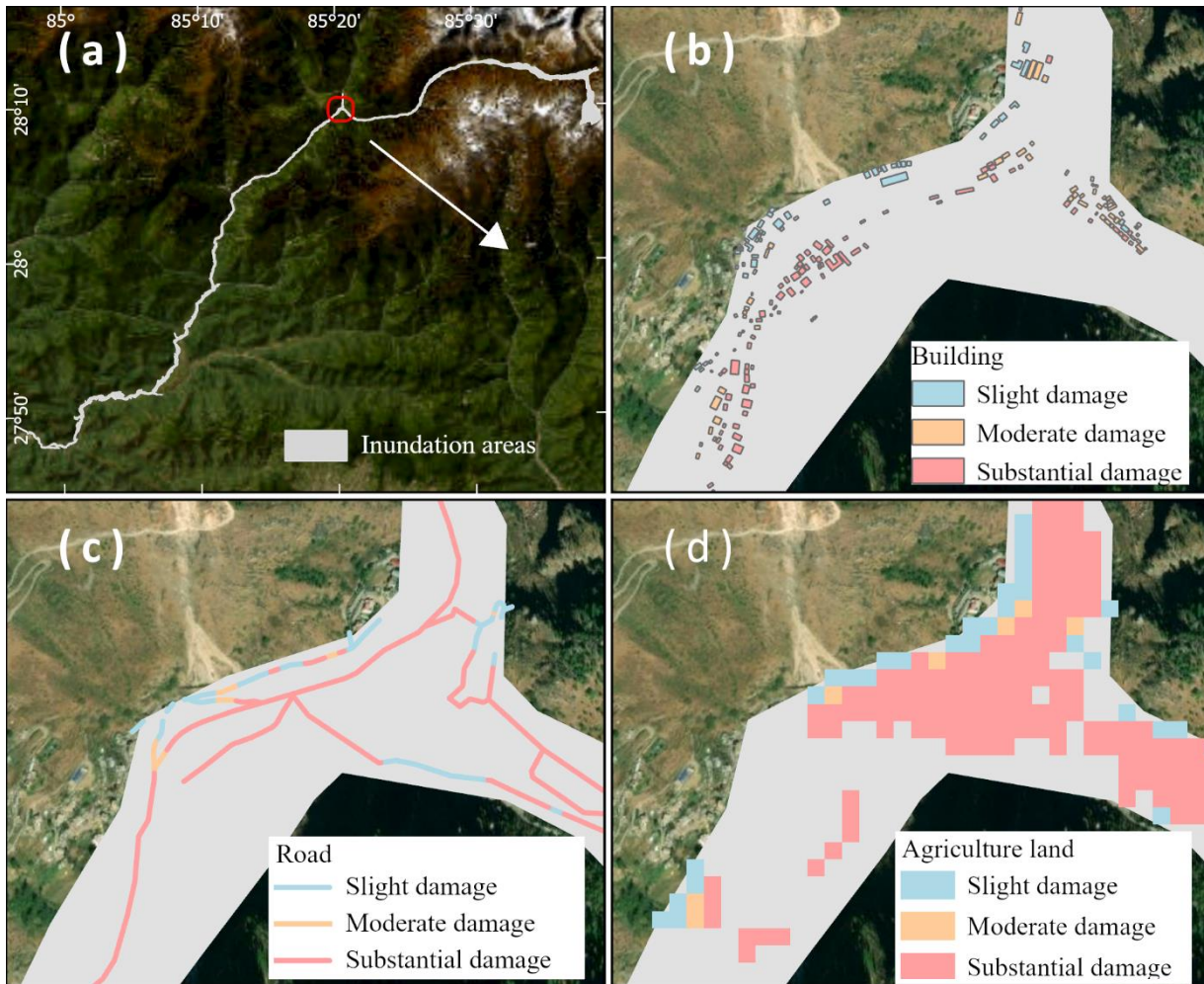
465 **Fig 8 Damage to buildings, roads, and agricultural land caused by the most serious GLOF due to Lake Anonymous 12**

5 Discussion

GLOFs can have a significant impact due to the large volume of water stored in glacial lakes, resulting in rapid breaches, high outflow peaks, and high total discharges. While there is a positive correlation between inundation extent and lake area (Fig 6), it's important to note that inundation propagation and extent also depend on dam breach processes as well as the underlying

470 topography and land surface conditions of downstream areas (Worni et al., 2012; Ancey et al., 2019). Particularly, steep and narrow valley gorges can influence flood waves, causing them to rapidly spread over long distances, often accompanied by significant physical processes such as erosion and the transport of ice, sediment, and debris. Among the 21 PDGLs in Nepal, Tsho Rolpa Lake, Thulagi Lake, and Lower Barun Lake are expected to experience the most severe impacts of GLOFs on buildings, roads and agricultural areas. Rounce et al. (2016, 2017) also assessed the downstream impacts of GLOFs from

glacial lakes in the Nepal Himalayas. They likewise identified Tsho Rolpa Lake, Lower Barun Lake, and Thulagi Lake as
having the most affected buildings, while two anonymous lakes and Thulagi Lake were anticipated to experience the most
significant impacts on agricultural areas. However, it's important to note that Rounce et al. (2016, 2017) employed the Monte
Carlo least-cost path model (Watson et al., 2015) to estimate the extent of GLOFs for each lake. While the model is
computationally efficient and suitable for large-scale applications, it lacks a physical basis and relies solely on the terrain
conditions downstream along the river channel, without considering variations in lake release volumes and peak discharges.
As a result, flood extents for lakes with differing potential flood volumes may be indistinguishable. Another limitation is that
the threshold for the cut-off distance in MC-LCP needs to be artificially set, while the realistic cutoff distance downstream for
each lake varies, sometimes extending over 200 km downstream (Richardson & Reynolds, 2000). This study takes a different
approach by employing a physics-based hydrodynamic model that predicts not only the inundation extent but also the spatial
characteristics of flood features, including inundation probabilities and water depth while considering various outburst
scenarios. This information can be used to identify potential exposures and assess the extent of damage to which exposures
may be subject.

In addition to the growing vulnerability of human settlements in mountainous regions, there is an increasing exposure of
infrastructure related to energy security and commerce to GLOFs. Therefore, an objective assessment of the risk to
infrastructure posed by PDGLs is crucial. This study considers hydropower plants, given their critical importance and rapid
development in Nepal. Nepal is at the heart of a modern resurgence in hydropower development in the Himalayas (Lord et al.,
2016). The country boasts abundant hydropower resources thanks to its ample river water, steep gradients, and mountainous
terrain. At present, a considerable number of hydropower projects are in the planning and construction stages (46 projects
exceeding 100 gigawatts) to enhance the country's overall generating capacity. These planned hydropower projects are
primarily situated along rivers connected to glaciers located in the northern region of Nepal (Shakti et al., 2021). While a few
existing hydropower plants have experienced direct impacts from recorded GLOFs, such as the Namche hydroelectric power
plant destroyed by the 1985 Dig Tsho GLOF (Vuichard & Zimmermann, 1987) and the Bhotekoshi hydropower plant affected
by the 2016 GLOF (Cook et al., 2018), GLOFs can be highly destructive and unpredictable, posing a significant threat to
hydropower facilities. Furthermore, the expansion of hydropower plants into the upstream regions of watersheds substantially
increases the vulnerability of infrastructure to GLOFs (Nie et al., 2021). Schwanghart et al. (2016) estimated that two-thirds
of the existing and planned hydropower projects in the Himalayas are located in areas potentially affected by GLOFs, and up
to one-third of these projects could face GLOF discharges exceeding their local design flood capacities. In this study, we have
identified 49 existing and planned hydropower projects that could potentially be impacted by GLOFs originating from the 21
PDGLs; however, we did not assess the specific impacts of GLOFs on these hydropower projects. To our knowledge, there
are no readily available damage curves that correlate the potential impact on hydropower plants with flood depth and other
flood characteristics. Furthermore, hydropower plants typically comprise multiple components, including the dam and
reservoir, powerhouse and auxiliary facilities, among others. The spatial extent of a hydropower plant can vary significantly,
ranging from a few square kilometres to several hundred square kilometres. Accurate assessment would require detailed spatial
information and mapping of hydropower plants, which is currently lacking. Consequently, this study focuses exclusively on
identifying whether a hydropower plant is potentially at risk from GLOFs, without engaging in a detailed assessment of the
specific damages that may be incurred. Still, we urge stakeholders responsible for planning, designing, constructing, and
managing infrastructure to consider these potential GLOF risks.

In addition to well-studied PDGLs like Tsho Rolpa Lake, Thulagi Lake, and Lower Barun Lake, some anonymous lakes also
present a significant risk of GLOFs. For instance, Anonymous 12, 1, 7, 11, 8, and 2 pose high GLOF risks. GLOFs from any
of these six lakes have the potential to impact more than 200 buildings, and GLOFs resulting from Lake Anonymous 12 may
submerge existing hydropower facilities. Unfortunately, there is limited information available about these anonymous lakes in

comparison to well-studied PDGLs. To gain a better understanding of their conditions, a comprehensive research strategy is needed, which includes fieldwork investigations, remote sensing techniques, and modelling approaches. This study has leveraged remote sensing techniques and modelling approaches to preliminarily identify PDGLs with a high level of exposure and potential impacts from GLOFs. However, it is imperative to conduct fieldwork investigations, including in situ measurements, to obtain the essential information required to comprehend the actual state of these anonymous lakes at the local scale. These field investigations will also serve as ground truth to calibrate remote sensing-based data and model outputs. Moreover, considering the challenging nature of fieldwork in glacial lake areas, the cost of expeditions, and the high level of fitness and expertise required by monitoring teams, the preliminary identification of PDGLs with high exposure and potential impacts can offer valuable evidence to support decision-making in the allocation of financial and human resources.

We acknowledge the importance of validating the proposed framework for estimating the impact of GLOFs while recognizing the inherent challenges associated with validation due to the limited availability of historical data. Although Nie et al. (2018), Veh et al. (2019), and Shrestha et al. (2023) have provided valuable inventories of historical GLOFs in the Himalayas, these primarily provide information on the date and location of outbursts, offering limited or no information on the actual impacts resulting from historical GLOFs. Even when impact data is available, it often comprises only generalized descriptions, encompassing metrics like the overall number of casualties, infrastructure damage, and affected villages, lacking specific spatial information. Consequently, obtaining adequate data for validating our proposed impact estimation framework for GLOFs proves challenging. It is noteworthy that our proposed framework employs the fully physically based hydrodynamic model HiPIMS, intricately designed to capture the highly transient and complex hydrodynamic processes induced by events such as dam breaks and flash floods. HiPIMS has been successfully validated for these extreme flow conditions (e.g., Smith and Liang, 2013; Liang et al., 2016). The adoption of this model enhances our confidence in simulating the spatial-temporal processes of GLOF inundation, ultimately contributing to improved hazard evaluation results. Furthermore, we employ Bayesian approaches to derive plausible value ranges for lake volumes and peak discharges. These approaches facilitate the creation of multiple GLOF scenarios for each glacial lake, ensuring comprehensive coverage of all potential glacial lake outburst scenarios. The incorporation of Bayesian methods allows us to account for uncertainties, thereby enhancing the robustness of our impact evaluation for potentially devastating GLOFs.

6 Conclusion

Exposure and damage estimations are integral components of GLOF risk assessment. Having sufficient information about the potential impacts of GLOFs originating from PDGLs is essential to facilitate GLOF risk management. In this study, we harnessed multi-temporal satellite imagery, Bayesian regression models that establish relationships between lake areas and depths, as well as between flood volume and peak discharge, and a high-performance hydrodynamic flood model to support GLOF exposure and damage assessments for multiple lakes. We applied this assessment framework to 21 PDGLs identified in the Nepal Himalaya, and the key findings of this study are summarized as follows:

- Utilizing multi-temporal imagery capturing different hydrological conditions of glacial lakes enables the derivation of the full or maximum glacial lake boundaries for potential risk assessment.

- The Bayesian regression model, which establishes relationships between lake areas and depths, as well as between flood volume and peak discharge, can produce predictive posterior distributions for lake depths and peak discharges for each lake. These distributions offer a plausible range of values for lake volumes and peak discharges for each PDGL, facilitating subsequent objective flood modelling and impact analysis.

555 • The hydrodynamic model (HiPIMS), supported by parallelized high-performance GPU computation, is capable of predicting the resulting GLOFs in terms of temporally and spatially varying flood frequency and water depths to reflect the highly transient flood dynamics under various scenarios for multiple glacial lakes on a large scale.

• Among the 21 PDGLs identified in the Nepal Himalayas, Tsho Rolpa Lake, Thulagi Lake, and Lower Barun Lake are poised to bear the most severe impacts of GLOFs on buildings, roads, and agricultural areas. Six anonymous lakes,

560 specifically Anonymous 12 (85°37′51″ E, 28°09′44″ N), Anonymous 1 (87°44′59″ E, 27°48′57″ N), Anonymous 7 (86°55′41″ E, 27°51′00″ N), Anonymous 11 (86°51′29″ E, 27°41′13″ N), Anonymous 8 (86°55′01″ E, 27°49′55″ N), and Anonymous 2 (87°56′05″ N, 27°47′26″ E), have the potential to impact more than 200 buildings. The GLOFs from these 21 PDGLs can also impact the 5 existing hydropower plants and the 44 hydropower projects that have been granted generation or survey licenses. Notably, Anonymous 12 may even submerge existing hydropower facilities.

565 **Appendix**: List of abbreviations used in this study.

CI	confidence interval
DEM	digital elevation model
EVI	Enhanced Vegetation Index
GIS	Geographic Information System
GLOFs	Glacial Lake Outburst Floods
GPU	Graphics processing unit
HDI	highest density interval
HiPIMS	High-Performance Integrated Hydrodynamic Modelling System
MNDWI	Modified Normalized Difference Water Index
NIR	Near Infrared
NDMI	Normalized Difference Moisture Index
NDVI	Normalized Difference Vegetation Index
NDWI	Normalized Difference Water Index
OSM	OpenStreetMap
PDGL	potentially dangerous glacial lake
SRTM	Shuttle Radar Topography Mission
TOA	Top-Of-Atmosphere

References

Ancey, C., Bardou, E., Funk, M., Huss, M., Werder, M. A., & Trewhela, T. (2019). Hydraulic reconstruction of the 1818 Giétro glacial lake outburst flood. *Water Resources Research*, 55(11), 8840-8863.

Arcement, G. J., & Schneider, V. R. (1989). Guide for selecting Manning's roughness coefficients for natural channels and

570 flood plains. Washington, DC: US Government Printing Office.

Bajracharya, S. R., Maharjan, S. B., Shrestha, F., Sherpa, T. C., Wagle, N., & Shrestha, A. B. (2020). Inventory of glacial lakes and identification of potentially dangerous glacial lakes in the Koshi, Gandaki, and Karnali River Basins of Nepal, the Tibet Autonomous Region of China. International Centre for Integrated Mountain Development GPO Box, 3226.

Barnes, H. H. (1967). Roughness characteristics of natural channels. US Government Printing Office.

575 Bishop, C. M., & Tipping, M. E. (2003). Bayesian regression and classification. *Nato Science Series sub Series III Computer And Systems Sciences*, *190*, 267-288.

Breiman, L. (2001). Random forests. *Machine learning*, 45(1), 5-32.

Budhathoki, K. P., Bajracharya, O. R., & Pokharel, B. K. (2010). Assessment of Imja Glacier Lake outburst flood (GLOF) risk in Dudh Koshi River Basin using remote sensing techniques. *Journal of Hydrology and Meteorology*, *7*(1), 75-91.

580 Chen, H., Liang, Q., Liang, Z., Liu, Y., & Ren, T. (2020). Extraction of connected river networks from multi-temporal remote sensing imagery using a path tracking technique. *Remote Sensing of Environment*, 246, 111868.

Chen, H., Zhao, J., Liang, Q., Maharjan, S. B., & Joshi, S. P. (2022). Assessing the potential impact of glacial lake outburst floods on individual objects using a high-performance hydrodynamic model and open-source data. *Science of The Total Environment*, 806, 151289.

585 Chow, V.T., (1959). Open-channel Hydraulics. Book Co., New York, McGraw-Hill, p.680.

Cook, K. L., Andermann, C., Gimbert, F., Adhikari, B. R., & Hovius, N. (2018). Glacial lake outburst floods as drivers of fluvial erosion in the Himalaya. *Science*, *362*(6410), 53-57.

Cook, S. J., & Quincey, D. J. (2015). Estimating the volume of Alpine glacial lakes. *Earth Surface Dynamics*, *3*(4), 559-575.

Dubey, S., & Goyal, M. K. (2020). Glacial lake outburst flood hazard, downstream impact, and risk over the Indian

590 Himalayas. *Water Resources Research*, *56*(4), e2019WR026533.

Ellison, A. M. (2004). Bayesian inference in ecology. *Ecology letters*, *7*(6), 509-520.

Farr, T. G., Rosen, P. A., Caro, E., Crippen, R., Duren, R., Hensley, S., ... & Alsdorf, D. (2007). The shuttle radar topography mission. *Reviews of geophysics*, 45(2).

FEMA. (2009). Multi-hazard loss estimation methodology: Flood model. HAZUS-MH MR3 technical manual. P220.

595 Gao, B. C. (1996). NDWI—A normalized difference water index for remote sensing of vegetation liquid water from space. *Remote sensing of environment*, *58*(3), 257-266.

Ghimire, M. (2004). Review of studies on glacier lake outburst floods and associated vulnerability in the Himalayas. *Himalayan Review*, 49-64.

Granshaw, F. D., & Fountain, A. G. (2006). Glacier change (1958–1998) in the north Cascades national park complex,

600 Washington, USA. *Journal of Glaciology*, *52*(177), 251-256.

Haritashya, U. K., Kargel, J. S., Shugar, D. H., Leonard, G. J., Strattman, K., Watson, C. S., ... & Regmi, D. (2018). Evolution and controls of large glacial lakes in the Nepal Himalaya. *Remote Sensing*, 10(5), 798.

Huete, A., Didan, K., Miura, T., Rodriguez, E. P., Gao, X., & Ferreira, L. G. (2002). Overview of the radiometric and biophysical performance of the MODIS vegetation indices. *Remote sensing of environment*, *83*(1-2), 195-213.

605 Huggel, C., Kääb, A., Haeberli, W., Teysseire, P., & Paul, F. (2002). Remote sensing based assessment of hazards from glacier lake outbursts: a case study in the Swiss Alps. *Canadian Geotechnical Journal*, *39*(2), 316-330.

Huizinga, J., De Moel, H., & Szewczyk, W. (2017). Global flood depth-damage functions: Methodology and the database with guidelines (No. JRC105688). Joint Research Centre (Seville site).

Kapitsa, V., Shahgedanova, M., Machguth, H., Severskiy, I., & Medeu, A. (2017). Assessment of evolution and risks of

610 glacier lake outbursts in the Djungarskiy Alatau, Central Asia, using Landsat imagery and glacier bed topography modelling. *Natural Hazards and Earth System Sciences*, *17*(10), 1837-1856.

Khadka, N., Zhang, G., & Chen, W. (2019). The state of six dangerous glacial lakes in the Nepalese Himalaya. TAO: Terrestrial, *Atmospheric and Oceanic Sciences*, 30(1), 6.

Krause, L., Mal, S., Karki, R., & Schickhoff, U. (2019). Recession of Trakarding glacier and expansion of Tsho Rolpa lake

615 in Nepal Himalaya based on satellite data. *Himalayan Geology*, 40(2), 103-114.

Lala, J. M., Rounce, D. R., & McKinney, D. C. (2017). Modeling the glacial lake outburst flood process chain in the Nepal Himalaya: reassessing Imja Tsho's hazard. *Hydrology and Earth System Sciences*, 22, 3721–3737

Lamsal, D., Sawagaki, T., Watanabe, T., & Byers, A. C. (2016). Assessment of glacial lake development and prospects of outburst susceptibility: Chamlang South Glacier, eastern Nepal Himalaya. *Geomatics, Natural Hazards and Risk*, 7(1), 403-423.

Land cover of Nepal 2010 http://rds.icimod.org/Home/DataDetail?metadataId=9224 (2020) Accessed 2020-04-26

Lord, A. (2016). Citizens of a hydropower nation: Territory and agency at the frontiers of hydropower development in Nepal. *Economic Anthropology*, 3(1), 145-160.

Liang, Q., Chen, K. C., Jingming, H. O. U., Xiong, Y., Gang, W., & Qiang, J. (2016). Hydrodynamic modelling of flow impact on structures under extreme flow conditions. *Journal of Hydrodynamics*, Ser. B, 28(2), 267-274.

McFeeters, S. K. (1996). The use of the Normalized Difference Water Index (NDWI) in the delineation of open water features. *International journal of remote sensing*, *17*(7), 1425-1432.

Mool, P. K., Maskey, P. R., Koirala, A., Joshi, S. P., Lizong, W., Shrestha, A. B., ... & Shrestha, R. B. (2011). Glacial lakes and glacial lake outburst floods in Nepal. https://policycommons.net/artifacts/1516291/glacial-lakes-and-glacial-lake-outburst-floods-in-nepal/2192662/. Accessed 2022-04-26

Morris, M. W., Hassan, M. A. A. M., & Vaskinn, K. A. (2007). Breach formation: Field test and laboratory experiments. *Journal of Hydraulic Research*, 45(sup1), 9-17.

Muñoz, R., Huggel, C., Frey, H., Cochachin, A., & Haeberli, W. (2020). Glacial lake depth and volume estimation based on a large bathymetric dataset from the Cordillera Blanca, Peru. *Earth surface processes and landforms*, *45*(7), 1510-1527.

Nepal Hydropower portal. (2019) Available at: https://hydro.naxa.com.np/core/about Accessed 22 August 2023.

Nie, Y., Liu, Q., Wang, J., Zhang, Y., Sheng, Y., & Liu, S. (2018). An inventory of historical glacial lake outburst floods in the Himalayas based on remote sensing observations and geomorphological analysis. *Geomorphology*, 308, 91-106.Nie, Y., Pritchard, H. D., Liu, Q., Hennig, T., Wang, W., Wang, X., ... & Chen, X. (2021). Glacial change and hydrological implications in the Himalaya and Karakoram. *Nature reviews earth & environment*, *2*(2), 91-106.

Nie, Y., Sheng, Y., Liu, Q., Liu, L., Liu, S., Zhang, Y., & Song, C. (2017). A regional-scale assessment of Himalayan glacial lake changes using satellite observations from 1990 to 2015. *Remote Sensing of Environment*, *189*, 1-13.

OpenStreetMap data for Nepal http://download.geofabrik.de/asia/nepal.html (2015) Accessed 2022-04-26

Rana, B., Shrestha, A. B., Reynolds, J. M., Aryal, R., Pokhrel, A. P., & Budhathoki, K. P. (2000). Hazard assessment of the Tsho Rolpa Glacier Lake and ongoing remediation measures. *Journal of Nepal Geological Society*, 22, 563.

Richardson, S. D., & Reynolds, J. M. (2000). An overview of glacial hazards in the Himalayas. *Quaternary International*, *65*, 31-47.

Rinzin, S., Zhang, G., Sattar, A., Wangchuk, S., Allen, S. K., Dunning, S., & Peng, M. (2023). GLOF hazard, exposure, vulnerability, and risk assessment of potentially dangerous glacial lakes in the Bhutan Himalaya. *Journal of Hydrology*, 619, 129311.

Rodriguez-Galiano, V. F., Ghimire, B., Rogan, J., Chica-Olmo, M., & Rigol-Sanchez, J. P. (2012). An assessment of the effectiveness of a random forest classifier for land-cover classification. *ISPRS journal of photogrammetry and remote sensing*, *67*, 93-104.

Rounce, D. R., McKinney, D. C., Lala, J. M., Byers, A. C., & Watson, C. S. (2016). A new remote hazard and risk assessment framework for glacial lakes in the Nepal Himalaya. Hydrology and Earth System Sciences, 20(9), 3455-3475.

Rounce, D. R., Watson, C. S., & McKinney, D. C. (2017). Identification of hazard and risk for glacial lakes in the Nepal Himalaya using satellite imagery from 2000–2015. *Remote Sensing*, *9*(7), 654.

Sattar, A., Goswami, A., & Kulkarni, A. V. (2019). Hydrodynamic moraine-breach modeling and outburst flood routing-A hazard assessment of the South Lhonak lake, Sikkim. *Science of the total environment*, *668*, 362-378.

Sattar, A., Haritashya, U. K., Kargel, J. S., Leonard, G. J., Shugar, D. H., & Chase, D. V. (2021). Modeling lake outburst and downstream hazard assessment of the Lower Barun Glacial Lake, Nepal Himalaya. *Journal of Hydrology*, *598*, 126208.

Scawthorn, C., Flores, P., Blais, N., Seligson, H., Tate, E., Chang, S., ... & Lawrence, M. (2006). HAZUS-MH flood loss estimation methodology. II. Damage and loss assessment. *Natural Hazards Review*, 7(2), 72-81.

Schaffer-Smith, D., Swenson, J. J., Barbaree, B., & Reiter, M. E. (2017). Three decades of Landsat-derived spring surface water dynamics in an agricultural wetland mosaic; Implications for migratory shorebirds. *Remote Sensing of Environment*, *193*, 180-192.

Schwanghart, W., Worni, R., Huggel, C., Stoffel, M., & Korup, O. (2016). Uncertainty in the Himalayan energy–water nexus: Estimating regional exposure to glacial lake outburst floods. *Environmental Research Letters*, *11*(7), 074005.

Shakti, P. C., Pun, I., Talchabhadel, R., & Kshetri, D. (2021). The Role of Glaciers in Hydropower Production in Nepal. *Journal of Asian Energy Studies*, 5(1), 1-13.

Shrestha, B. B., & Nakagawa, H. (2014). Assessment of potential outburst floods from the Tsho Rolpa glacial lake in Nepal. *Natural Hazards*, *71*(1), 913-936.

Shrestha, F., Steiner, J. F., Shrestha, R., Dhungel, Y., Joshi, S. P., Inglis, S., ... & Zhang, T. (2023). A comprehensive and version-controlled database of glacial lake outburst floods in High Mountain Asia. *Earth System Science Data*, *15*(9), 3941-3961.

Shugar, D. H., Burr, A., Haritashya, U. K., Kargel, J. S., Watson, C. S., Kennedy, M. C., ... & Strattman, K. (2020). Rapid worldwide growth of glacial lakes since 1990. *Nature Climate Change*, *10*(10), 939-945.

Somos-Valenzuela, M. A., McKinney, D. C., Byers, A. C., Rounce, D. R., Portocarrero, C., & Lamsal, D. (2015). Assessing downstream flood impacts due to a potential GLOF from Imja Tsho in Nepal. *Hydrology and Earth System Sciences*, *19*(3), 1401-1412.

Smith, L. S., & Liang, Q. (2013). Towards a generalised GPU/CPU shallow-flow modelling tool. *Computers & Fluids*, 88, 334-343.

Somos-Valenzuela, M. A., McKinney, D. C., Rounce, D. R., & Byers, A. C. (2014). Changes in Imja Tsho in the Mount Everest region of Nepal. *The Cryosphere*, *8*(5), 1661-1671.

Tucker, C. J. (1979). Red and photographic infrared linear combinations for monitoring vegetation. *Remote sensing of Environment*, *8*(2), 127-150.

Tulbure, M. G., Broich, M., Stehman, S. V., & Kommareddy, A. (2016). Surface water extent dynamics from three decades of seasonally continuous Landsat time series at subcontinental scale in a semi-arid region. *Remote Sensing of Environment*, *178*, 142-157.

Veh, G., Korup, O., von Specht, S., Roessner, S., & Walz, A. (2019). Unchanged frequency of moraine-dammed glacial lake outburst floods in the Himalaya. *Nature Climate Change*, 9(5), 379-383.

Veh, G., Korup, O., & Walz, A. (2020). Hazard from Himalayan glacier lake outburst floods. *Proceedings of the National Academy of Sciences*, 117(2), 907-912.

Vuichard, D., & Zimmermann, M. (1987). The 1985 catastrophic drainage of a moraine-dammed lake, Khumbu Himal, Nepal: cause and consequences. *Mountain Research and Development*, 91-110.

Walder, J. S., Iverson, R. M., Godt, J. W., Logan, M., & Solovitz, S. A. (2015). Controls on the breach geometry and flood hydrograph during overtopping of noncohesive earthen dams. *Water Resources Research*, 51(8), 6701-6724.

Walder, J. S., & O'Connor, J. E. (1997). Methods for predicting peak discharge of floods caused by failure of natural and constructed earthen dams. *Water Resources Research*, 33(10), 2337-2348.

Watson, C. S., Carrivick, J., & Quincey, D. (2015). An improved method to represent DEM uncertainty in glacial lake outburst flood propagation using stochastic simulations. *Journal of Hydrology*, *529*, 1373-1389.

Worni, R., Huggel, C., & Stoffel, M. (2013). Glacial lakes in the Indian Himalayas—From an area-wide glacial lake inventory to on-site and modeling based risk assessment of critical glacial lakes. *Science of the Total Environment*, *468*, S71-S84.

Worni, R., Stoffel, M., Huggel, C., Volz, C., Casteller, A., & Luckman, B. (2012). Analysis and dynamic modeling of a moraine failure and glacier lake outburst flood at Ventisquero Negro, Patagonian Andes (Argentina). *Journal of Hydrology*, *444*, 134-145.

Xu, H. (2006). Modification of normalised difference water index (NDWI) to enhance open water features in remotely sensed imagery. *International journal of remote sensing*, *27*(14), 3025-3033.

Yang, M., Cai, Q., Li, Z., & Yang, J. (2023). Uncertainty analysis on flood routing of embankment dam breach due to overtopping failure. *Scientific Reports*, 13(1), 20151.

Yang, Y., Cao, S. Y., Yang, K. J., & Li, W. P. (2015). Experimental study of breach process of landslide dams by overtopping and its initiation mechanisms. *Journal of Hydrodynamics*, 27(6), 872-883.

Yu, X., Hyyppä, J., Vastaranta, M., Holopainen, M., & Viitala, R. (2011). Predicting individual tree attributes from airborne laser point clouds based on the random forests technique. *ISPRS Journal of Photogrammetry and remote sensing*, *66*(1), 28-37.

Zhang, G., Yao, T., Xie, H., Wang, W., & Yang, W. (2015). An inventory of glacial lakes in the Third Pole region and their changes in response to global warming. *Global and Planetary Change*, *131*, 148-157.

Zhao, J., & Liang, Q. (2022). Novel variable reconstruction and friction term discretisation schemes for hydrodynamic modelling of overland flow and surface water flooding. *Advances in Water Resources*, 163, 104187.

Zhang, T., Wang, W., & An, B. (2023a). A conceptual model for glacial lake bathymetric distribution. *The Cryosphere Discussions*, 2023, 1-35.

Zhang, T., Wang, W., An, B., & Wei, L. (2023b). Enhanced glacial lake activity threatens numerous communities and infrastructure in the Third Pole. *Nature Communications*, 14(1), 8250.

Zheng, G., Allen, S. K., Bao, A., Ballesteros-Cánovas, J. A., Huss, M., Zhang, G., ... & Stoffel, M. (2021). Increasing risk of glacial lake outburst floods from future Third Pole deglaciation. *Nature Climate Change*, *11*(5), 411-417.

Data availability

The DEM used in this work is the SRTM DEM. Land use types are extracted from the Landsat TM imagery from the year 2010, which can be accessed at http://rds.icimod.org/Home/DataDetail?metadataId=9224.The OpenStreetMap (OSM) data can be accessed via the link http://download.geofabrik.de/asia/nepal.html. Hydropower plant data are obtained from the Hydro Map project through the link https://hydro.naxa.com.np/core/about.

Code availability

The flood model can be accessed through the link https://github.com/HEMLab/HiPIMS-CUDA.

Author contribution

HC was responsible for developing the methodology, conducting analysis, and drafting the paper. QL handled funding acquisition, research design, and reviewing and refining the draft. JZ developed the flood model codes, and SM provided a review of the draft.

Competing interests

The contact author has declared that none of the authors has any competing interests.

Acknowledgments

740 This work is supported by the WeACT project (NE/S005919/1) funded by the UK Natural Environment Research Council (NERC) through the SHEAR programme.